DEVELOPMENT OF A TEST RIG TO STUDY THE LUBRICATING OIL DEGRADATION AND SOLID DEPOSIT FORMATION PROCESS AT HIGH TEMPERATURES

A Thesis

by

RAQUEL JUAREZ FUNEZ

Submitted to the Office of Graduate and Professional Studies of
Texas A&M University
in partial fulfillment of the requirements for the degree of

MASTER OF SCIENCE

Chair of Committee,	Eric L. Petersen
Committee Members,	Oliver Mathieu
	Chad Mashuga
Head of Department,	Bryan Rasmussen

May 2021

Major Subject: Mechanical Engineering

ABSTRACT

Over the last several decades, turbine efficiency has improved significantly, resulting in higher turbine operating temperatures that negatively affect the lubricating oil circulating through the system. Exposure to high temperatures results in oil degradation and the eventual formation of solid deposits in the oil which greatly limit the oil's ability to reduce wear and cool the turbine components. An experimental apparatus was designed and built to allow for the studying and better understanding of this phenomenon.

The apparatus consists of a flow loop with a heated test section through which the oil is pumped. The oil that comes into contact with the hot surfaces degrades and forms solid deposits. As time passes, the deposit buildup decreases the heat transfer that occurs at the test section. The bulk oil temperatures into and out of the test section are used as indicators of the deposit induction time and buildup rate, and the deposits may be analyzed at the end of the experiment. Air or an inert gas may be used to pressurize the system to up to 1,000 psi, while test section surface temperatures may be as high as 650°C. Full details of the design, construction, and validation of the new facility are provided in this thesis.

Data of one of the initial tests performed with the apparatus are included. During the test, SuperTech's conventional SAE 5W-30 motor oil was exposed to surface temperatures of up to 595°C and then returned to the main reservoir. The system was pressurized with nitrogen at 25 psig (39.61 psi). The test resulted in the clear formation of solid deposits on the heated surfaces and in data that show the decrease in the bulk oil

temperature over time due to their formation. Assembly and testing of the apparatus have been completed, and it is now fully operational and ready for future studies on lubricating oil thermal degradation and oxidation.

ACKNOWLEDGMENTS

I would like to thank my advisor, Dr. Petersen, for the opportunity to work on this project, and for his guidance, support, and patience as I completed it. I would also like to thank Dr. Mathieu for his support throughout this process, and Dr. Mashuga for serving on my thesis committee.

Thanks also go to Mr. Carl Johnson at the TEES Turbomachinery Laboratory for his help and patience while machining parts, and to *all* my lab colleagues and friends for their advice, time, kindness, and willingness to help.

Finally, thanks to my parents for their guidance, support, and prayers during my years as an undergraduate and graduate student.

CONTRIBUTORS AND FUNDING SOURCES

Contributors

This work was supervised by a thesis committee consisting of Professors Eric L. Petersen and Oliver Mathieu of the Department of Mechanical Engineering and Professor Chad Mashuga of the Department of Chemical Engineering.

All work conducted for the thesis was completed by the student, under the advisement of Dr. Eric L. Petersen of the Department of Mechanical Engineering.

Funding Sources

Graduate study was supported by the Petersen research group within the TEES Turbomachinery Laboratory, and by the Texas A&M Engineering Experiment Station (TEES).

NOMENCLATURE

HLPS	Hot Liquid Process Simulator
PFRU	Portable Fouling Research Unit
rpm	Revolutions per minute
FEA	Finite element analysis
T	Temperature
P	Pressure

TABLE OF CONTENTS

Page

ABSTRACT ii

ACKNOWLEDGMENTS iv

CONTRIBUTORS AND FUNDING SOURCES v

NOMENCLATURE vi

TABLE OF CONTENTS vii

LIST OF FIGURES ix

LIST OF TABLES xi

1. INTRODUCTION 1

2. LITERATURE REVIEW 3

2.1. Lubricating Oil Composition 3
2.2. Mechanism of Coke Formation 5
2.2.1. Oxidation 7
2.2.2. Thermal Decomposition 13
2.3. Previous Test Rigs 15
2.3.1. Penn State Micro Oxidation Test 16
2.3.2. Panel Coker Test 17
2.3.3. Hot Liquid Process Simulator 17
2.3.4. Portable Fouling Research Unit 18

3. TEST RIG DESIGN 20

3.1. General Design 20
3.2. Test Rig Components 22
3.2.1. Valves, Fittings and Tubing 23
3.2.2. Bottom Reservoir 25
3.2.3. Bottom Reservoir Stand 26
3.2.4. Pump 27
3.2.5. Flow Meter 29
3.2.6. Test Section 30

3.2.7. Band Heater 30
3.2.8. Top Reservoir 32
3.2.9. Top Reservoir Clamps 32
3.2.10. Pressure Transducers 33
3.2.11. Thermocouples 35
3.2.12. Pressure and Temperature Display and Data Acquisition 36
3.2.13. Panels and Frame 36
3.3. Completed Apparatus 38
3.4. Extreme Temperatures and Pressure Ratings 39

4. TESTING 43

4.1. Pressure Testing 43
4.2. Oil Testing 44

5. CONCLUSIONS 50

5.1. Summary 50
5.2. Future Work 51

REFERENCES 52

APPENDIX A STANDARD OPERATING PROCEDURE 55

APPENDIX B LIST OF SOME OF THE ITEMS USED FOR TEST RIG ASSEMBLY 58

APPENDIX C MELT PRESSURE TRANSDUCER ADAPTOR FEA ANALYSIS RESULTS 61

APPENDIX D HEAT TRANSFER ANALYSIS 62

APPENDIX E PART DRAWINGS 66

LIST OF FIGURES

Page

Figure 1 Sample of coke deposits. Reprinted from ExxonMobil [4]. 5

Figure 2 Oil degradation process of a thin layer of lubricating oil on a hot surface [13]. 7

Figure 3 Varnish on an inlet guide vane valve. Reprinted from Fitch and Gebarin [18]. 8

Figure 4 Sludge formed from lubricating oil. Reprinted from Livingstone et al.[23]. 8

Figure 5 Penn State Micro Oxidation Test apparatus [17]. 16

Figure 6 Panel Coker Test apparatus [36]. 17

Figure 7 Hot Liquid Process Simulator apparatus [38]. 18

Figure 8 Coking test rig component layout and main components. 21

Figure 9 Test rig tubing function definition. Red tubing carries oil only, while blue tubing carries gases only. The valves with the high-temperature extension are marked in yellow. 24

Figure 10 Bottom reservoir mounted on its stand. 27

Figure 11 Mahr spinning pump unit and motor. 28

Figure 12 Variable-frequency drive for pump. 28

Figure 13 Flow meter mounted to the test rig's front panel. 29

Figure 14 Test section tubing with machined cones and threads. 30

Figure 15 Test section with tubing adaptors, resistance band heaters, thermocouples, and insulation 31

Figure 16 Top reservoir mounted onto the front panel. 32

Figure 17 Melt pressure transducer and adaptor installed on a hiP tee. 34

Figure 18 Gas manifold pressure transducer and cooling element. 35

Figure 19 Inlet and outlet thermocouple assembly. 36

Figure 20 Final test rig with stainless steel front panel and polycarbonate back and side panels.....38

Figure 21 Assembled test rig components. 39

Figure 22 Temperature traces for SuperTech conventional motor oil SAE 5W - 30 with a surface temperature of 595 °C. 46

Figure 23 Deposits formed in test section for SuperTech conventional motor oil SAE 5W - 30 with a surface temperature of 595 °C. (a) and (b) show the deposits still in the test section tubing (c) shows the deposits collected after removal from the test section.....47

Figure 24 Temperature traces for Mobil DTE 732 turbine oil with a surface temperature of 475 °C.....48

LIST OF TABLES

Page

Table 1 Common additives and their main functions [12]. 5

Table 2 Test rig design considerations. 21

Table 3 Bottom reservoir pressure rating at elevated temperatures [42]. 26

Table 4 Temperature derating factors for 316 stainless-steel components. 40

Table 5 Test rig component pressure ratings at elevated temperatures. 42

Table 6 Maximum allowable stress at various temperatures for 316 stainless steel. 43

Table B1 Items used in the test rig supplied by the High Pressure Equipment Company. 58

Table B2 Items used in the test rig supplied by Omega Engineering. 59

Table B3 Items used in the test rig supplied by various manufacturers. 60

Table D1 Fluid properties used in heat transfer calculations [46]. 65

Table D2 Length of tubing required for oil to cool down from T_1 = 550°C to T_2 at various flow rates. 65

1. INTRODUCTION

Gas turbine technology has improved over the last several decades. The greater efficiencies and advanced engine materials result in higher turbine operating temperatures which, in turn, negatively affect the lubricating oil circulating throughout the system [1]. In fact, gas turbines produce the most severe turbine oil operating conditions, when compared to water and steam turbines, due to high sump temperatures and high hot-spot peaks [2, 3]. Exposing lubricating oils to extreme temperatures results in the formation of solid deposits in the oil, or, more specifically, in coke formation. Coke deposits are insidious, black, solid, carbonaceous deposits formed as a result of oil oxidation and thermal breakdown at extreme engine temperatures [1, 4, 5]. The formation of solid deposits greatly limits the oil's ability to reduce wear and cool the turbine components. In addition, coke formation is a major cause of premature component failure; results in high maintenance costs and valves sticking; interferes with heat transfer from the parts to the oil; reduces oil flow rates; and clogs tubes and nozzles that spray lubricants on the bearing [2, 5, 6].

Since progress towards higher-efficiency turbines, and therefore higher operating temperatures, will continue, and since turbine operators want to extend the periods between maintenance as far as possible, gaining an understanding of the high-temperature oil degradation and solid deposit formation process is necessary. Although the search for answers is decades long, the existing investigations have not resulted in concrete solutions, and further research is still necessary. Several bench tests exist to evaluate an oil's ability

to resist oxidation and thermal degradation. However, most of both the standardized tests used by oil manufacturers and other tests developed over time do not meet the temperatures or conditions experienced by the oils in operation. For example, the Rotating Pressure Vessel Oxidation Test (RPVOT) and Turbine Oil Stability Test (TOST), two ASTM standardized tests used by oil manufacturers, only reach temperatures of 150°C and 95°C, respectively [7, 8]; on the other hand, according to previous studies, coke formation can occur at hotspots at more than 400°C in supply lines during operation or at 300°C in static oil films after engine shutdown [2, 6]. There is therefore a need for a test rig that is able to test the oils under conditions that more closely resemble real-life turbine oil operating conditions. This thesis describes the development and characterization of such an apparatus.

Provided first is a literature review that discusses lubricating oil composition, the oxidation and thermal decomposition process, and previous test rigs. A detailed description of the test rig and its components' functions and pressure and temperature ratings follows. Finally, information on the initial tests and results obtained is included.

2. LITERATURE REVIEW

Despite the need for a solution to the oil degradation problem that exists in several areas of industry, the available information about this phenomenon is limited. There is some information available, however, on the coking process, oxidation and the factors affecting it, and thermal breakdown of lubricating oils. The following section provides a summary.

2.1. Lubricating Oil Composition

Most engine oils are composed of a basestock or base oil (72-96%) that is formed by hydrocarbons and is commonly obtained through either the refining of crude oil or through synthetic formation, and an additive package (4-28%) [9]. The base oil provides the fluid layer that separates moving surfaces, reduces friction, and removes heat and wear particles while the additives enhance or create properties in the base oil [10]. The base oil must be able to keep all the additives in solution at all times under normal operating conditions.

The American Petroleum Institute (API) classifies the base oil types into five groups. The base oils are mostly classified based on sulfur and saturate concentration and viscosity-index range. However, a more general description is provided here. Base oils in Groups I, II, and III are derived from crude oil and are therefore considered as mineral based. Group IV oils are polyalphaolefins (PAOs) only, which are chemically synthesized oils [10-12]. Group V base oils include all base stocks that do not fall under the other categories and include both mineral-based and synthetic oils [10-12].

Group I oils are made from traditional, simpler solvent refining techniques and are the least expensive, the least molecularly uniform, and have the lowest operating temperature range [10-12]. Group II and III base oils are both produced by hydroprocessing [12]. They have better antioxidant properties, have a clearer color and are more expensive when compared to Group I oils [11]. Group III base oils are more refined and purer than those in Group II [10, 11]. Group IV includes the chemically synthesized PAOs and have "a unique combination of high temperature viscosity retention, low volatility, very low pour point, and a high degree of oxidation resistance" [12]. Finally, Group V base oils are also chemically engineered and include all oils that do not fall into the other groups. Like those in Group IV, they have several advantages over the base oils in the first three groups [11]. The lines between these categories are becoming less clear as the refining processes evolve [10].

Additives are chemical compounds added to lubricating oils to impart specific properties, enhance already existing properties, or reduce the rate at which undesirable changes progress [12]. Table 1 provides a summary of some of the most common additives and their main functions. Although additives greatly improve the performance of lubricating oils, excessive amounts or unwanted interactions between additives may yield negative side effects [12]. Oil manufacturers, therefore, search for the right balance and combination of base oils and additives to obtain the best results and must test for the negative side effects. Understanding the base stocks and additives available and how they interact with each other, and matching their behavior with the machine's needs and operating conditions is necessary to obtain the best performance [12].

Table 1 Common additives and their main functions [12].

Additive	Main Function
Pour Point Depressants	Lower the temperature at which rigid wax crystal structures that impede flow form.
Viscosity Index Improvers	Increase the viscosity of the oil at high temperatures. Prevent it from thinning out.
Antioxidants	Decrease the oxidation rate, increasing the service life. Depleted as they perform their job.
Detergents	Neutralize deposit precursors.
Dispersants	Disperse potential deposit forming materials in the oil.

2.2. Mechanism of Coke Formation

Coke is an insidious, black, solid, carbonaceous deposit that is formed from the degradation of lubricating oil at extremely high temperatures [1, 4]. Figure 1 contains a picture of coke deposits.

Figure 1 Sample of coke deposits. Reprinted from ExxonMobil [4].

Kauffman et al. [13] described the oil degradation process for a thin layer of oil on a hot surface which is illustrated in Fig. 2. The process is as follows: The antioxidants protect the base oil but are depleted as time passes. This protection continues until the ineffective antioxidant level, here defined as 10% of the original antioxidant package, is reached. The time at the high temperature required to reach the ineffective antioxidant level is called the induction time. Next, the basestock esters begin to polymerize and form intermediate oligomers that remain dissolved in the oil. Esters are molecules that are formed by the reaction of an alcohol with an acid, and they are the main components of synthetic oils [14]. An oligomer is a type of polymer; unlike a polymer, however, it is made of only a few monomers (the basic units that form a polymer) and is, therefore, lighter. The oxidation is inhibited by the antioxidants at first but proceeds rapidly once they have been depleted. Weight loss in this stage also indicates that more-volatile molecules are also forming. In the third step, "the polymers grow large enough to become insoluble in the oil", resulting in the initial deposits. The final step, in which the polymers turn into coke, does not require oxygen but speeds up the process.

Kauffman et al. [13] also make several statements about the process that stand out. First, antioxidants delay the coke formation process. Second, although the addition of antioxidants increases induction time, it also increases the amount of deposit formed once coking takes place. Third, "if the time that a thin oil layer spends on a hot surface at elevated temperatures can be limited so that the antioxidant does not deplete completely, coking can be prevented" [13]. Oil choice (including antioxidant package choice) makes

a difference on how long this time can be. Finally, the surface material does not affect the rate of antioxidant depletion, but it does affect the polymer and coke formation rate.

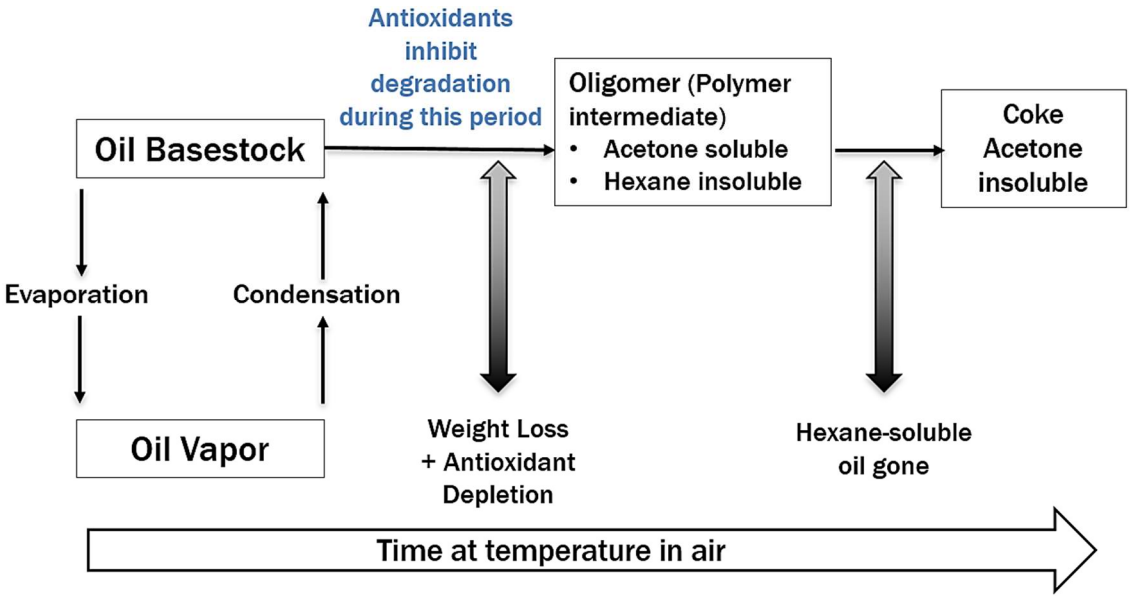

Figure 2 Oil degradation process of a thin layer of lubricating oil on a hot surface [13].

2.2.1. Oxidation

Many list oxidation as the main form of lubricant degradation [15-17]; but, in the literature that discusses the oxidation of lubricating oils (as opposed to coke formation), sludge and varnish, rather than coke, are mentioned as the direct result of the oxidation process. Figure 3 and Fig. 4 show images of varnish and sludge, respectively. "Varnish is typically distinguished as a thin, insoluble, nonwipeable film deposit, whereas sludge is soft and tacky and can move about the system" [18]. However, several papers, including the one discussed in the previous section, state that oxidation is an important part of the coke formation process and/or that antioxidants prevent coke formation [1, 4-6, 12, 13, 19-22]. Pirro et al. [12] provide an explanation to this seeming discrepancy: "In extreme

cases, these deposits [sludge, varnish and lacquer] may be further oxidized to form hard, carbonaceous materials ” (i.e. coke) [12].

Figure 3 Varnish on an inlet guide vane valve. Reprinted from Fitch and Gebarin [18].

Figure 4 Sludge formed from lubricating oil. Reprinted from Livingstone et al.[23].

The general steps of oxidation and deposit formation are described below. Here, R represents a hydrocarbon and R· represents a hydrocarbon with a free radical. A free radical is formed when a covalent bond breaks and “one electron remains with each of the fragments” [24]. “Free radicals are electrically neutral, but because of their unpaired electrons, are usually highly reactive” [24].

1. The initiation reactions involve the formation of free radicals [9, 15, 16, 25, 26]. Reactions 1, 2, and 3 show examples of reactions that lead to free radical formation.

$$RH \xrightarrow[heat,light,catalyst]{} R\cdot + H \quad (1)$$

$$RH + O_2 \rightarrow R\cdot + HOO\cdot \quad (2)$$

$$2RH + O_2 \rightarrow 2R\cdot + H_2O_2 \quad (3)$$

2. Alkyl radicals (R·) in the lubricant react with the dissolved oxygen (O_2) in the high-temperature air to produce peroxy radicals (ROO·) [5, 9, 10, 15, 16, 25-27].

$$R\cdot + O_2 \rightarrow ROO\cdot \quad (4)$$

3. The peroxy radicals react with additional hydrocarbon molecules to form hydroperoxides (ROOH) [5, 10, 15, 26, 28, 29] and additional alkyl radicals [5, 26]. This step (Reaction 5), along with Reaction 4, is called the propagation step [5, 9, 10, 15, 25, 26].

$$ROO\cdot + RH \rightarrow ROOH + R\cdot \quad (5)$$

4. "A variety of chain branching steps are possible based on the lubricant type and system temperature" [26]; some of these are shown in Reactions 6 through 8 [5, 10, 15, 16, 25, 26].

$$ROOH \rightarrow RO\cdot + HO\cdot \quad (6)$$

$$RO\cdot + RH \rightarrow ROH + R\cdot \quad (7)$$

$$HO\cdot + RH \rightarrow H_2O + R\cdot \quad (8)$$

5. The two reactions most relevant to sludge formation are the decomposition of the hydroperoxide to form low molecular weight (LMW) materials such as aldehydes and ketones [10, 15-17, 25-29]. Two of the most accepted mechanisms of their formation are shown in Reactions 9 and 10 [5, 26].

$$RR'HCO\cdot \rightarrow RCH=O+R'\cdot \quad (9a)$$

$$RR'R"CO\cdot \rightarrow RR'C=O+R"\cdot \quad (9b)$$

$$2RR'CHOO\cdot \rightarrow R'RC=O+RCHOHR'+O_2 \quad (10)$$

6. The oxidation reactions also produce alcohols and acids [10, 15-17, 25-29]. The aldehydes, ketones, alcohols, and acids are called the primary oxidation products. Reaction 10 is an example of alcohol formation during oxidation. Reactions 7 and 8 show an alkoxy radical (RO·) and hydroxy radical (HO·) removing a hydrogen atom from another hydrocarbon and producing alcohols and water, respectively [26]. "Carboxylic acids are formed by oxidation of aldehydes and ketones" [26].

7. Polymerization or condensation of the primary oxidation products leads to the formation of high molecular weight (HMW) materials which increase the viscosity and have a limited solubility in the un-oxidized components of the lubricant and therefore precipitate as lacquers, varnishes, or sludges [5, 10, 15-17, 25-29].

Aldol condensation reactions play a significant role in this step once high levels of aldehydes and ketones have been formed [5, 26, 29]. Aldol condensation reactions are studied in organic chemistry, and they are "a useful way of joining two carbon chains together" [30]. Bakunin and Parenago [29], however, state that aldol condensation reactions are unlikely, and name the Knoevenagel-type condensation reaction, a modification of the Aldol condensation reaction [31] as a reasonable alternative.

2.2.1.1. Temperature Dependence

Oxidation will gradually occur under mild operating conditions, but temperature is the primary catalyst of all oxidation reactions [18, 32]. There is a rule of thumb that for every 10°C increase in operating temperature, the rate of oxidation doubles (Arrhenius Rate Rule) [9, 12, 18]. Although Zerla and Moore [27] state that a 10°C change in temperature at the temperatures they tested caused the induction time to change by approximately 1.5 times only.

2.2.1.2. Catalysts

Metallic elements present in the lubricating oil generally act as catalysts and speed up the degradation process. Iron, copper, lead, and aluminum in particular are described in the literature as oxidation catalysts [4, 15, 18, 25, 26, 28, 33]. Although these metals are the ones typically mentioned in the literature, they "are probably no worse in their effect than several others which could act as catalysts, such as manganese, chromium, or vanadium, but they play a more important role because of their much greater prevalence" [33]. The oxidation initiation reactions catalyzed by iron and copper are illustrated in Reactions 11 and 12 [5, 26].

$$Fe^{3+} + ROOH \rightarrow Fe^{2+} + ROO\cdot + H^{+} \quad (11a)$$

$$Fe^{2+} + ROOH \rightarrow Fe^{3+} + RO\cdot + HO^{-} \quad (11b)$$

$$Cu^{2+} + ROOH \rightarrow Cu^{+} + ROO\cdot + H^{+} \quad (12a)$$

$$Cu^{+} + ROOH \rightarrow Cu^{2+} + RO\cdot + HO^{-} \quad (12b)$$

It is important to point out that, in general, oils can "tolerate" small amounts of catalysts without any significant negative effects, but once the catalyst concentration

increases beyond a certain point, the increase in catalyst concentration will decrease the induction period; if the concentration increases even more, a point "where the system is again insensitive to further change in concentration" is reached again [33]. Light and water may also act as oxidation catalysts [3, 9, 18, 25].

2.2.1.3. Antioxidants

Antioxidants play an important role in preventing oxidation [9, 10, 16, 26, 28, 33] and, therefore, deposit formation [6, 13, 26, 27]. Antioxidants act in different ways to control the degradation of lubricants:

- Radical scavengers (primary antioxidants): "function to scavenge alkyl peroxy and alkoxy radicals before they can react with oil molecules in the propagation reactions" [5, 9, 10, 26]; they prevent Reaction 5 from occurring and cause Reaction 13 to occur instead where $A\cdot$ is the antioxidant radical [10, 16, 26].

$$ROO\cdot + AH + RH \rightarrow ROOH + A\cdot + RH \quad (13)$$

- Peroxide decomposers (secondary antioxidants): "decompose the unstable alkyl hydroperoxides to the more stable alcohol form" [5, 10, 16, 26]. They prevent initiation Reactions 11 and 12 and propagation Reactions 6, 7, and 8 from occurring [26].
- Metal deactivators: act as "metal passivators to prevent catalytic effects" that lead to oxidation initiation [5, 9, 16].

Lubricants respond differently to different additives, and their response is affected by several factors such as temperature, metal contamination, the materials that make up the equipment, and the chemical composition of the basestock [9, 26]. In addition, "certain

combinations of antioxidants exhibit a stabilization synergy that cannot be achieved when using the antioxidants individually", and that synergy is also dependent on the previously mentioned factors [10, 26]. Also, note that antioxidants are depleted as they perform their job; no antioxidant remains in the lubricant during the entire lifetime of the oil.

There are tradeoffs to using antioxidants. If coke does form, "a higher initial antioxidant level will probably produce a larger deposit than would be obtained with a lower antioxidant level" [6, 13]. To meet the original equipment manufacturers' requirements for turbine oils, oil developers use "higher additive treat rates" that, due to the limited solvency of synthetic base stocks and the vulnerable thermal stability of some antioxidants, can cause additive dropout, sludge, and varnish at early stages of use [2]. Therefore, ideally, an oil should have an optimal ratio of the different kinds of antioxidants that has synergistic potential and lowers the needed additive treat rates [2].

2.2.2. Thermal Decomposition

"Thermal stability, as opposed to oxidation stability, is the ability of an oil or additive to resist decomposition under prolonged exposure to high temperatures with minimal oxygen present" [12]. Very little information about this second path of lubricating oil degradation, thermal decomposition, is currently found in the literature. Wiehe [34] shares a kinetic model to describe "coke formation during the thermolysis of petroleum residua" that may give some clues on the process that lubricating oils undergo, summarized below:

1. "Asphaltenes have a thermally stable, polynuclear aromatic core with saturate and aromatic pendants" that are thermally cracked to form free radicals.

Saturates and aromatics are the nonpolar and lighter fractions of crude oil, while resins and asphaltenes are the polar, heavier, and nonvolatile fractions, asphaltenes being the heaviest and most polar [35].

2. The residua contain natural donors that donate hydrogen and terminate free radicals.
3. The solubility of asphaltenes decreases as they lose pendants and approach the reaction limit of the asphaltene aromatic core. Eventually, "the asphaltenes become insoluble in the reacting medium and undergo a liquid-liquid phase separation to form a phase lean in hydrogen donors". This phase separation is the end of the induction period.
4. It is in this heavy phase that "the asphaltene free radicals combine by addition and recombination reactions to form high molecular-weight coke".

The oil can reach the temperatures required for thermal decomposition by coming into contact with a hot surface, due to adiabatic compression from entrained bubbles, or due to an electrostatic discharge.

- Machine surfaces with temperatures greater than 200°C result in thermal degradation, depending on the oil [18].
- Adiabatic compression from entrained bubbles occurs when air bubbles travel from low pressure to high pressure. The pressure change causes the bubble to implode which results in an "intense entrapment of the heat and extreme rise in temperature locally in the oil" (above 1000°F may be reached) [18]. Pressure-induced dieseling (PID) is a special situation that occurs "when fluids are aerated

and high compression pressures are experienced". "The temperature reached with PID leads to microscopic ignition (called partial combustion) of the oxygen-rich oil vapors" [18].

- Electrostatic discharge is caused by the electrostatic charge generation and subsequent static discharging that causes temperature increases and thermal-oxidative oil degradation. Temperatures as high as 10,000 to 20,000°C may be reached [18].

2.3. Previous Test Rigs

The test rigs that have been developed to study the oil degradation and coking phenomenon can be classified into three general categories: static oil, heated plate, and flowing oil experiments. A general description of the categories is as follows.

- Static oil experiments: The oil sample is exposed to a high temperature, catalysts, and air or nitrogen. Samples are removed at regular intervals or at the end of the test for analysis.
- Heated-plate experiments: The oil is in contact with a heated plate, and the plate is analyzed for deposit weight and appearance.
- Flowing oil experiments: The heated oil flows through the system, and deposits are inspected at the end of the test.

Over a dozen experiments may be found in the literature, a few of them are described below.

2.3.1. Penn State Micro Oxidation Test

In this test, a cup made of low-carbon-steel (designed so that the oil will form a thin film on the metal surface) is placed at the bottom of the reactor (glass tube) which is then immersed in a constant-temperature bath [17]. Note that the low-carbon-steel is a catalyst for oxidation and polymerization reactions. Once the system is in equilibrium, the lubricant is injected into the cup. Air or nitrogen flows through the reactor for a specified amount of time [6]. When the test is finished, the cup is removed from the heating chamber, allowed to cool, and re-weighed to determine the weight of the remaining oil residue. The residues are then analyzed. Results are often reported as percent deposit of the oil injected [27]. Some authors have modified this test to improve repeatability and reduce test time and also developed less-costly alternatives [6, 27]. Figure 5 shows a picture of the apparatus used.

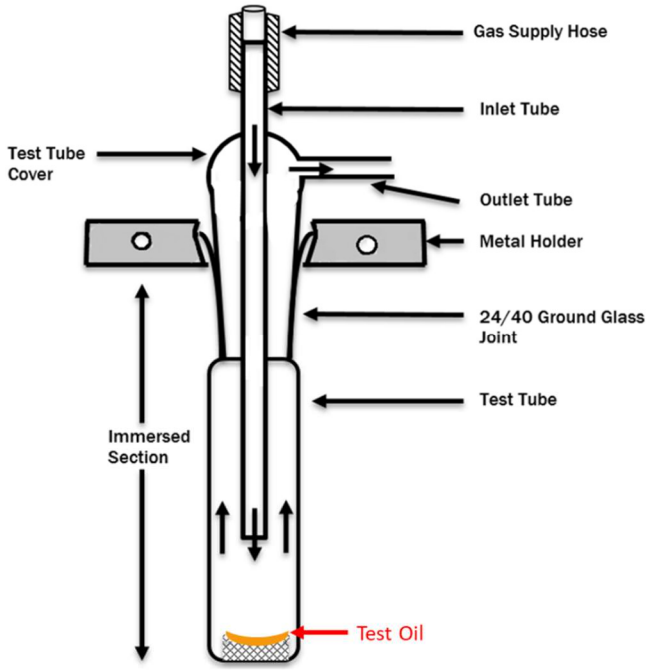

Figure 5 Penn State Micro Oxidation Test apparatus [17].

2.3.2. Panel Coker Test

The Panel Coker Test [22, 36, 37], in Fig. 6, consists of intermittently splashing the oil onto a heated, inclined "test panel under a cycle of 15 seconds operation and 45 seconds shutdown" [36]. The panel is inside a glass chamber in a humid air or other atmosphere. "At the end of the test, the nature and quantity of the deposits formed are evaluated" and the oil is analyzed for degradation [37].

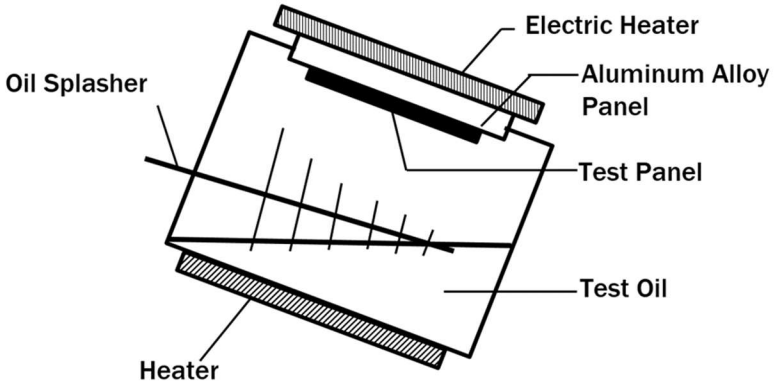

Figure 6 Panel Coker Test apparatus [36].

2.3.3. Hot Liquid Process Simulator

The hot liquid process simulator (HLPS) tests an "oil's propensity to form deposits in a fully flooded region of the engine"; it simulates oil flowing through pressurized lines [4, 10, 38]. The apparatus, which is similar to a heat exchanger, is sold by Alcor. In this test, the flow, pressure, and target surface temperature are selected [38]. Inlet and outlet temperatures as well as the axial profile of the surface temperature are recorded at different time intervals [38]. As fouling occurs, the heat flow to the fluid decreases, resulting in a decrease in the outlet fluid temperature [38]. The fouling resistance or fouling percentage versus time may be used to analyze coking propensity.[39]

The apparatus has a reservoir with a capacity of approximately 900 mL, a pressure rating of up to 1,000 psi, and a maximum test section surface temperature of 550°C [39]. The oil flow rate may be varied between 0.1 and 10 mL/min [39]. The oil may be recirculated several times through the test section (recirculation) or passed over the hot surface only once (one-shot or single pass). The test section consists of the oil flowing over an electrically heated tube with a constant surface temperature, shown in Fig. 7.

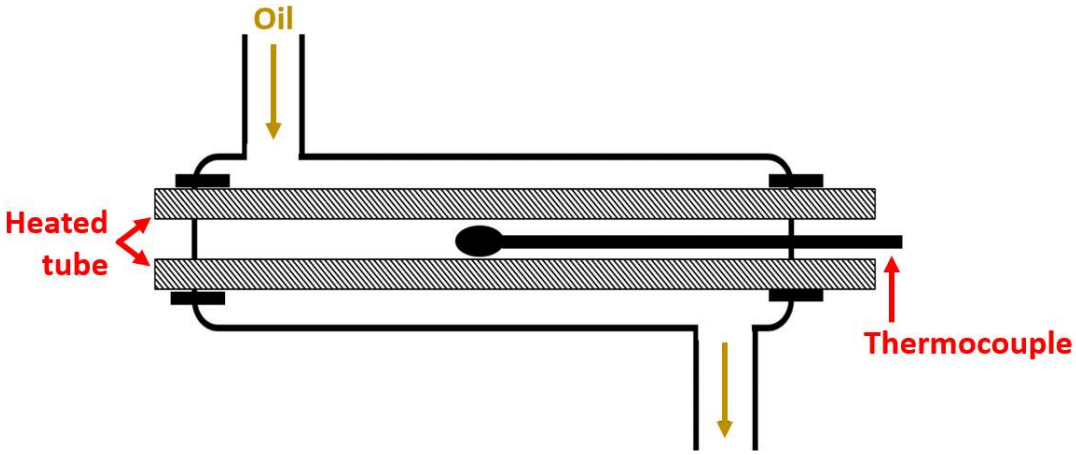

Figure 7 Hot Liquid Process Simulator apparatus [38].

2.3.4. Portable Fouling Research Unit

The Portable Fouling Research Unit (PFRU) is similar to the HLPS but larger; it is typically used to study crude oil fouling [38, 40, 41]. It operates at flow rates of around 4,830 mL/min; pressures between 145 and 194 psi under a nitrogen atmosphere; and a maximum design surface temperature at the test section of 630°C, although testing was done at lower temperatures (initial surface temperatures between 300°C and 380°C and bulk oil temperatures between 200°C and 285°C) [38, 40, 41]. Its tank has a capacity of 7.5 L of oil, and the oil circles back into the tank after passing through the test section.

The test section is similar to that of the HLPS, but under conditions of constant heat flux (rather than constant surface temperature).

3. TEST RIG DESIGN

3.1. General Design

Based on the information summarized in the previous chapter, the parameters that should be controlled, measured and varied in the test rig and between experiments were determined. The test rig should allow the researcher to control the time the oil is exposed to high temperatures, the surface temperature to which the oil is exposed, and the oil's flowrate, pressure, and level of exposure to oxygen. Similar to the experiments described in the literature, the deposits' appearance and weight, the induction time, and the deposit formation rate may be the parameters measured each experiment and used to analyze the degradation process. Finally, the rig should allow for the study of different kinds of lubricating oils with different basestocks, additives and antioxidant type and quantity.

Figure 8 shows the layout of this project's test rig with its main components. Before an experiment, the oil is inserted into the system with a syringe through the valve right above the bottom reservoir, and the whole system is pressurized with a gas. During an experiment, the oil is pumped out of the bottom reservoir, through a flow meter, through a heated test section, and is then sent back to the bottom reservoir or into the top reservoir. More details on the experimental procedure may be found in Appendix A Standard Operating Procedure. Table 2 summarizes the test rig's ratings and operating information.

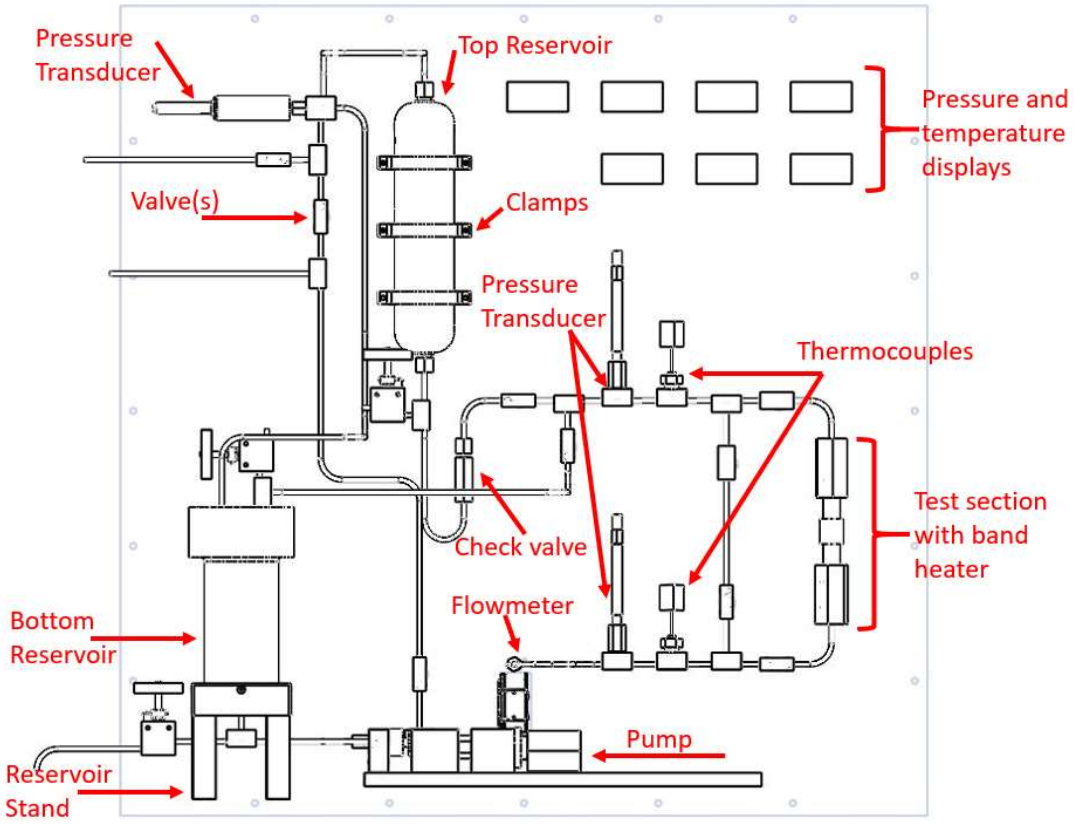

Figure 8 Coking test rig component layout and main components.

Table 2 Test rig design considerations.

Parameter	**Description**
Maximum system pressure	1,000 psi
Maximum test section surface temperatures	650°C
Maximum bulk oil temperature	550°C
Flow rate	< 15 mL/min
Pressurizing gas	Standard air (oxidation) or nitrogen (thermal decomposition)
Flow mode	Single pass or recirculation

The maximum system pressure was selected to match that of previously existing test rigs (the HLPS [39]) while also covering the range of desired applications, such as gas turbine engines. The maximum test section surface temperature surpasses that of any of the oil deposit test rigs currently found in the literature. The maximum possible bulk oil temperature was determined to be 100°C lower than the maximum test section surface temperature based on the findings of Srinivasan and Watkinson [40] when testing crude oil fouling in the PFRU. Very low oil flow rates were selected to shorten the required test times since, based on Srinivasan and Watkinson's studies [38, 40], higher velocities decrease the fouling rate perhaps since the oil spends less time in contact with the extreme-temperature surface. The pressurizing gas may be standard air to study the oxidation process, or nitrogen to study thermal decomposition only. Directing the oil back into the bottom reservoir (re-circulation mode) allows for the same oil to circulate several times past the test section, simulating how lubricating oils are typically used in the field. The oil may also be directed into the top reservoir (single-pass mode) if the effect of the oil encountering a hot surface only once is being studied.

3.2. Test Rig Components

A description of the test rig components shown in Fig. 8 above follows below. The components include the valves, fittings and tubing used to guide the oil flow; the reservoirs used to store the oil; the test section surface heaters; the pump; measuring devices such as thermocouples, pressure transducers, and flow meters; and other minor components. Their functions, and pressure and temperature ratings are discussed in detail.

3.2.1. Valves, Fittings and Tubing

All valves, fittings, adapters and tubing were supplied by the High Pressure Equipment Company (hiP). All tees used are made of 316 stainless steel and are rated for 20,000 psi at room temperature. The tubing used throughout the test rig is also made of 316 stainless steel, with a 0.25-inch outer diameter, 0.109-inch inner diameter, and a 20,000-psi pressure rating at room temperature. It is used for both the lines that carry the oil and the lines that compose the gas manifold used to pressurize the system. Figure 9 defines which tubing lines are meant to carry oil and which carry gases. The oil lines guide the oil from the bottom reservoir, through the pressure transducers, thermocouples and test section and back into the bottom reservoir, or into the top reservoir. A line that bypasses the test section was also installed. The gas lines form a gas manifold that is used to pressurize or vent the bottom and top reservoirs and to introduce a small amount of gas into the oil line if desired.

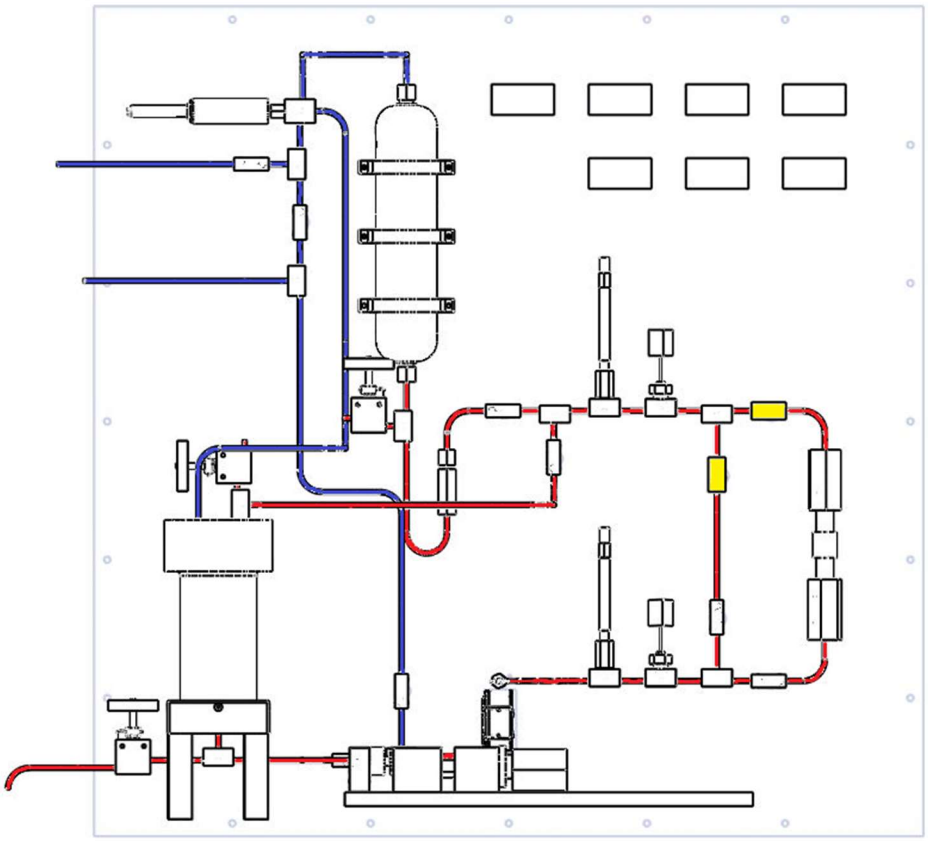

Figure 9 Test rig tubing function definition. Red tubing carries oil only, while blue tubing carries gases only. The valves with the high-temperature extension are marked in yellow.

The valves used are rated for 20,000 psi; they are made of 316 stainless steel and have Grafoil packing which increases their temperature rating to 427°C (800°F). In addition, two of the thirteen valves have extended stuffing boxes, which remove the packing area from the hot zone of the valve, making them suitable for 538°C (1,000°F). These two valves were placed at the point where the oil will experience the highest bulk temperatures; they are marked in Fig. 9. The hiP valves were selected because of these exceptionally high temperature and pressure ratings, not common among other high-pressure valve manufacturers, and because they result in very high safety factors even at

elevated temperatures. Finally, a ball check valve below the top reservoir prevents the oil from flowing back into the test section and is also rated for 20,000 psi.

All parts supplied by hiP use cone and threaded connections to seal since they withstand higher pressures and temperatures than other connection types. Adapters are therefore needed to connect to the flowmeter and top reservoir that use 0.25-inch and 0.5-inch NPT connections, respectively. These adapters are also made from 316 stainless steel and are rated for 15,000 psi at room temperature. Finally, the adapters that connect the 0.25-inch outer diameter tubing to the 1-inch tubing of the current test section are rated for 20,000 psi at room temperature.

Appendix B contains a list of the items and part numbers purchased from hiP that are used in the test rig. Drawings of the components used in the rig may be found in Appendix E.

3.2.2. Bottom Reservoir

The bottom reservoir is a bolted closure reactor that was manufactured by hiP. It is made of 316 stainless steel with a copper gasket. It has a one-liter capacity, three cone-and-threaded connections (two on top, one on the bottom), and a thermowell for a 0.0626-in thermocouple. The bottom connection leads to the pump inlet. One of the top connections is for the oil to return to the reservoir when the test rig is in re-circulation mode and to insert the oil into the system before an experiment. The second top connection is used to pressurize the reservoir. Table 3 lists the reservoir's pressure ratings at different temperatures.

Table 3 Bottom reservoir pressure rating at elevated temperatures [42].

Temperature		Pressure	Temperature		Pressure
°F	°C	Rating (psi)	°F	°C	Rating (psi)
100	38	5250	700	371	4900
200	93	5250	750	399	4800
300	149	5100	800	427	4200
400	204	5050	850	454	3400
500	260	5050	900	482	2500
600	316	5050	950	510	1700
650	343	5000	1000	538	900

3.2.3. Bottom Reservoir Stand

The bottom reservoir stand was machined to accommodate the connection at the bottom of the hiP reservoir. It was made from 6061 aluminum using the CNC machine in the Turbomachinery Laboratory. The reservoir is secured to the stand with two, 3/8-16 bolts that screw into the bottom of the reservoir. The stand legs are attached to the base with 1/4-20 bolts and may also be attached to the plate below them. Drawings of both the stand base and legs may be found in Appendix E. A picture of the bottom reservoir on its stand may be seen in Fig. 10.

Figure 10 Bottom reservoir mounted on its stand.

3.2.4. Pump

The pump is an integral part of the system; it promotes the flow of oil without the need of a pressure difference. However, finding a pump on the market that can withstand the high-pressure and -temperature conditions and still operate at low flow rates was not an easy task. Mahr's spinning pump was a great balance between withstanding the harsh conditions while operating at low flow rates. The pump's highest operating temperature and counter pressure are 350°C and 4,270 psi, respectively. The pump's recommended speed is 10 – 80 rpm. In this range, the pump's capacity is 1.6 – 13 mL/min. The flowrate is variable with the pump speed via the variable-frequency drive (VFD). The pump's inlet and outlet connections were adapted to match hiP's cone-and-threaded connections used throughout the system. Drawings of the pump unit and drive may also be found in

Appendix E, and Fig. 11 and Fig. 12 show pictures of the pump unit and motor and the pump's VFD, respectively.

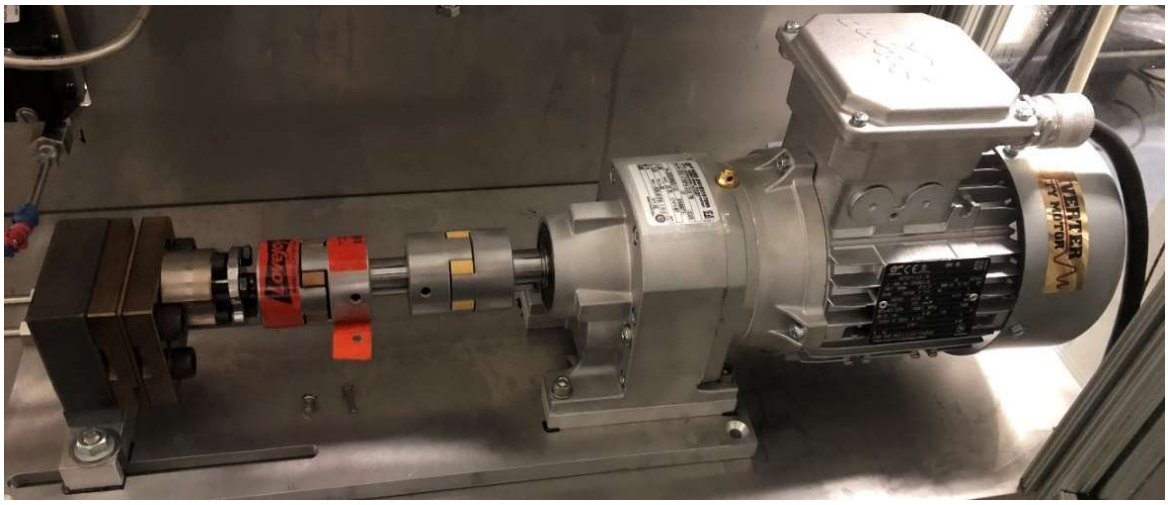

Figure 11 Mahr spinning pump unit and motor.

Figure 12 Variable-frequency drive for pump.

3.2.5. Flow Meter

All wetted parts of the flow meter are 316L stainless steel which enables it to withstand higher pressures and temperatures than the typical rotameter. Brooks Instrument's model MT3750 metal tube flow meter is ideal for the measurement of low flow rates and difficult-to-handle fluids (in this case, due to the high temperatures). It can measure flow rates in the range of 1.8 – 18 mL/min for a fluid with a specific density of 0.8527 and viscosity of 5.06 cP and can withstand temperatures and pressures of up to 204°C (400°F) and 4,000 psig, respectively. The inlet and outlet require 1/4-inch FNPT connections. Figure 13 shows a picture of the flow meter.

Figure 13 Flow meter mounted to the test rig's front panel.

3.2.6. Test Section

The current test section consists of a 316 stainless steel tube with a 1.00-inch outer diameter, 0.562-inch inner diameter, and length of 8- 9/16 in. The tube is rated for 20,000 psi and has coned-and-threaded ends that attach to two, 1/4-to-1-inch hiP adaptors (see Fig. 14). The cones and threads at both ends of the tubing were machined in a lathe in the machine shop at the Turbomachinery Laboratory. The test section tube is heated from the outside using two resistive band heaters. It is in this tube that the highest surface and bulk temperatures are located, and where the solid deposits form.

If the interest of the oil deposit studies changes, the test section geometry may be changed to something that more closely resembles the scenario of interest. The change of test section can simply be made by disconnecting the tubing from the valves just before and after the test section.

Figure 14 Test section tubing with machined cones and threads.

3.2.7. Band Heater

The current test section geometry uses two nozzle band heaters, supplied by Omega Engineering, to electrically heat the test section tubing. The stainless steel, resistive band heaters can reach temperatures as high as 760°C (1,400°F) and a power

density of up to 62 W/in^2. They are 1.5 inches long each, and clamp around the 1-inch outer diameter tubing. The test section temperature and/or heater output is regulated using a temperature controller. Thermocouples are placed in the heater's gap and held in place by its tightening screws and by the insulation wrapped around it. These thermocouples are connected to the temperature controller, the front panel meter and to the data acquisition device. The insulation must be wrapped around the heater only when the operating temperatures are below 649°C (1200°F) to avoid damaging the heater. Figure 15 shows the fully assembled test section with all of its components.

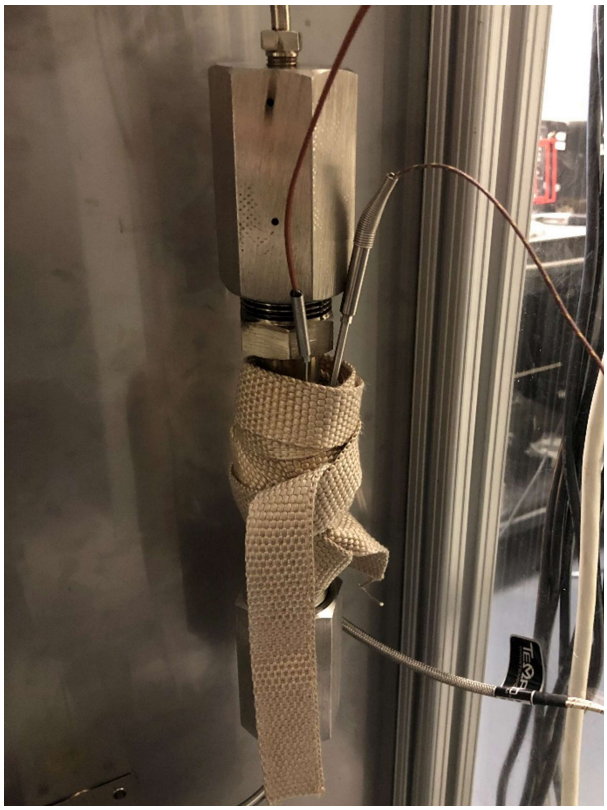

Figure 15 Test section with tubing adaptors, resistance band heaters, thermocouples, and insulation

3.2.8. Top Reservoir

The top reservoir is a sampling cylinder manufactured by Hoke. The cylinder is made of 316 stainless steel and has a one-liter capacity and a 5,000-psi pressure rating at room temperature. It has two, 1/2-inch NPT connections. The top connection connects to the gas manifold and is used to pressurize the cylinder. The bottom connection is used to fill and drain the oil from the reservoir.

3.2.9. Top Reservoir Clamps

The top reservoir is secured to the front panel with three clamps. These clamps were made of 6061 aluminum using the CNC machine at the Turbomachinery Laboratory. Each clamp is secured to the stainless-steel panel with two, 5/16-18 bolts. Appendix E contains a drawing of the clamps. Figure 16 shows the top reservoir mounted on the panel with the clamps.

Figure 16 Top reservoir mounted onto the front panel.

3.2.10. Pressure Transducers

Pressure transducers were placed before and after the test section to measure any pressure losses that may occur due to the deposit buildup. Melt pressure transducers were selected for this task as they are especially equipped to handle the high oil temperatures that they may encounter, unlike more-common transducers. The selected melt pressure transducers, supplied by MPI, can measure pressures as high as 1,500 psi at temperatures of up to 538°C (1,000°F). They have an inconel diaphragm and inconel threads, a 0.25% accuracy, and a 6-inch stem followed by an 18-inch flexible capillary with stainless steel armour that further isolates the transducers and allows for easier installation.

The tip of the MPI transducer does not have a typical cone-and-threaded or NPT connection and therefore required the machining of a special adaptor to connect it to the system. The adaptors simulate the 1/4-inch coned-and-threaded tubing on one end and have the openings and threads needed to connect the melt pressure transducers on the other end. They were made from 316/316L stainless steel using a lathe. The adaptors' pressure rating is 6,680 psi at room temperature; this was determined by running a finite element analysis on the part on SolidWorks, the results of which are found in Appendix C. Figure 17 shows the melt pressure transducer and the adaptor installed on a hiP fitting. Appendix E contains the drawing of the adaptors.

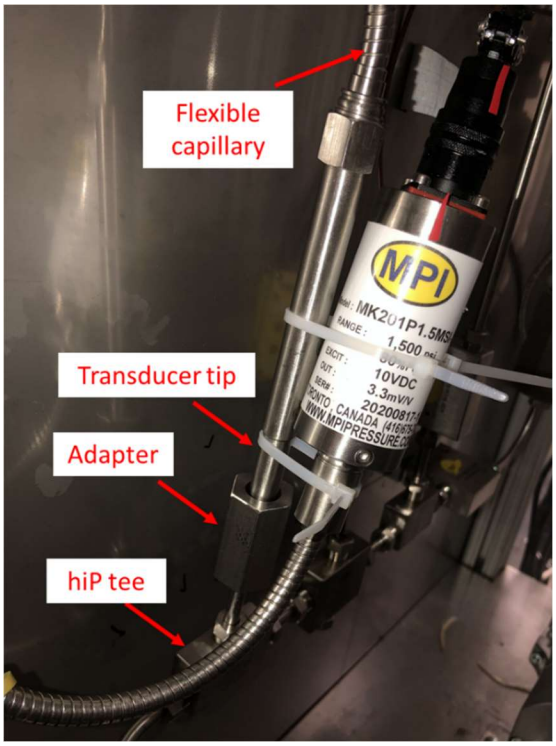

Figure 17 Melt pressure transducer and adaptor installed on a hiP tee.

There is a third pressure transducer installed in the gas manifold. This transducer is used to measure the pressures of the gas in the two reservoirs. Since the gas manifold will not reach temperatures as high as that of the oil, a melt pressure transducer was not used here. Instead, an Omega pressure transducer with a pressure range of 0 to 1,500 psig and an accuracy of ±0.08% was selected. The transducer's temperature compensation range, the temperature range within which the accuracy promised is valid, is only -29 to 85°C (-20 to 185°F). Although the temperatures in the gas manifold are lower than those in the oil, a cooling element was installed before the pressure transducer to help protect it from high fluid temperatures. The cooling element is rated for 10,000 psi at 300°C and is able to cool a fluid from 300°C to 25°C. The transducer and cooling element are shown in Fig. 18.

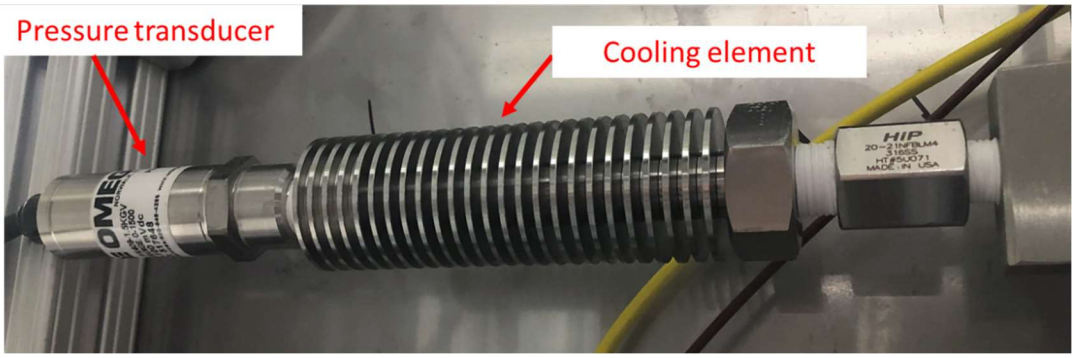

Figure 18 Gas manifold pressure transducer and cooling element.

3.2.11. Thermocouples

Type K thermocouples have been placed in four areas of the test rig. A dual thermocouple is placed in the thermowell at the top of the bottom reservoir; one set of wires is used to display the temperature on the displays in front of the rig, while the second set is wired to the data acquisition system to record the temperature readings for the duration of the test. It gives an estimate of the temperature of the oil in the reservoir to confirm that the oil going through the flowmeter and pump is not too hot. Two thermocouples are placed between the heater and the test section tubing. One thermocouple is used along with the temperature controller to maintain the desired test temperature, while the other is used to record and display the readings. Two more dual thermocouples are used to measure the temperature of the oil at the test section inlet and outlet, respectively. These TCs are also wired to both display and record the temperature readings. Since these thermocouples need to measure the oil temperature directly, they were installed into a tee using the assembly shown in Fig. 19.

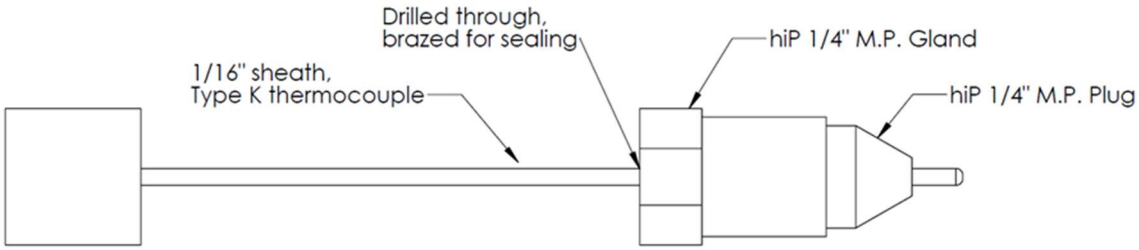

Figure 19 Inlet and outlet thermocouple assembly.

3.2.12. Pressure and Temperature Display and Data Acquisition

As mentioned above, the pressures and temperatures are measured and are both displayed on the front panel of the test rig and recorded for future analysis. Seven panel meters are used for the real-time temperature and pressure displays, while DATAQ's DI-2008 Thermocouple and Voltage Data Acquisition System with 8 channels is used for data recording.

3.2.13. Panels and Frame

All test rig components were arranged and enclosed behind stainless steel and polycarbonate panels and supported by aluminum T-slotted framing. In the unlikely case a component fails due to overly high pressures, the shields will protect the user and any bystanders. In addition, the shields enclose all high-temperature surfaces and protect against any injuries due to moving parts.

Baum [43] states that when a pressure vessel ruptures, the expanding fluid contents do work in fracturing the vessel, displacing the atmosphere and accelerating the fragments. Only a relatively small fraction (<20%) of the available work is transferred to a missile/fragment. The author provides equations to approximate the fragment velocity after a cylindrical pressure vessel rupture. Some of these equations are listed below, where

Equations 15 and 16 are for the cases of a single, small fragment and disintegration into many small fragments, respectively. Here, P_0 is the rupture pressure, A the projected area of the vessel wall that became a fragment, R the vessel radius, M the fragment mass, and a_0 the velocity of sound in the undisturbed high-pressure gas. The required thickness of the blast shield to prevent fragment perforation is given by Equation 17 where C_1, α, and β are empirical constants (with values of 6.523, 0.906, and -0.963, respectively, for stainless steel) [44]; t is the thickness measured in cm; V is the fragment velocity in m/s; m is the fragment mass in kg; A is the projected area of the fragment in cm^2; and F is the dimensionless initial acceleration of the fragment.

$$F = \frac{P_o A R}{M a_o^2} \tag{14}$$

$$\frac{V}{a_0} = \left[2F\left(\frac{h}{R}\right)\right]^{0.5} + 0.96\left[F\left(\frac{r}{R}\right)\right]^{0.25} \tag{15}$$

$$V = 0.88F^{0.55}a_0 \tag{16}$$

$$t = \left[\frac{V}{0.3048 \times 10^{C_1}(15432.4\ m)^{\beta}}\right]^{1/\alpha} (0.061024\ A)^{-1} \tag{17}$$

These equations were used to estimate the front panel thickness based on the bottom reservoir dimensions and a rupture pressure of 1,000 psi and air as the pressurizing gas. Both the single, small fragment and the disintegration equations indicated that a 0.036-inch-thick stainless-steel panel can protect against the largest fragment within the respective equation's limits. A 0.048-inch stainless-steel front panel was chosen. All other sides face areas that will not be accessed during experiments, but they are protected by 0.22-inch-thick polycarbonate panels, nonetheless.

The front panel also supports the rig components. A Jet Edge Waterjet was used to make cutouts on the panel for the valves, flow meter, top reservoir clamps, and panel meters.

3.3. Completed Apparatus

The frame and panels on the assembled test rig may be seen in Fig. 20, while the back of the test rig, with all its main components is shown in Fig. 21.

Figure 20 Final test rig with stainless steel front panel and polycarbonate back and side panels.

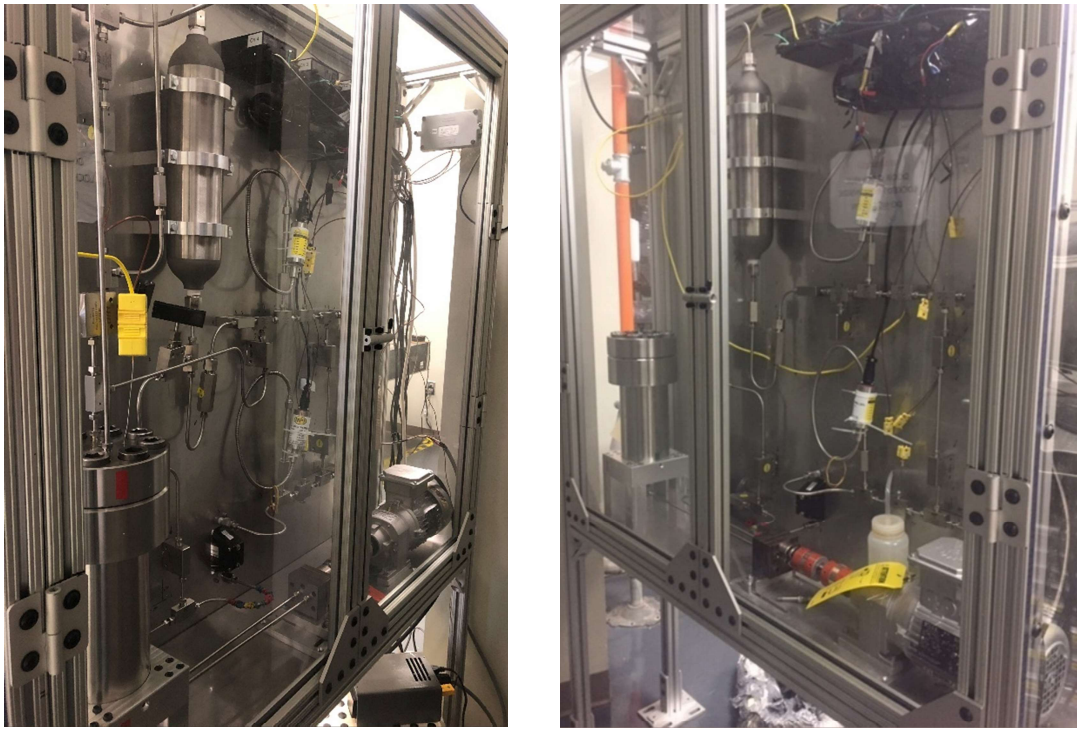

Figure 21 Assembled test rig components.

3.4. Extreme Temperatures and Pressure Ratings

The high temperatures involved in the experiment reduce the pressure rating of each component to a fraction of its value at room temperature. Temperature derating factors indicate what percentage of the pressure rating at room temperature remains at higher temperatures; they are given for a specific material and provided by manufacturers. Table 4 shows the temperature derating factors for 316 stainless steel provided by two manufacturers. Although all valves, fittings, and tubing were supplied by hiP (and not Parker), the derating factors supplied by Parker were used for higher temperatures since they were not supplied by hiP. This approach should be acceptable since the factors are material dependent only, and a comparison at lower temperatures shows agreement

between the factors supplied by both manufacturers. Table 3 shows pressure ratings of the bottom reservoir (hiP Bolted closure reactor) at various temperatures.

Table 4 Temperature derating factors for 316 stainless-steel components.

Temperature		**Derating Factor**	
°F	°C	hiP [42]	Parker [45]
300	149	100	100
400	204	96.5	97
500	260	90	90
600	316	85	85
650	343	83	--
700	371	81.5	82
750	399	80.5	--
800	427	79.5	80
850	453	78.5	--
900	486	--	78
1000	538	--	77
1100	593	--	62
1200	649	--	37

The maximum test section surface temperature that will be used is 650°C (~1200°F). According to previous, similar experiments, the highest temperature the oil can reach is 100°C below the test section surface temperature [40]. Therefore, the highest possible bulk oil temperature is 550°C (1022°F). Table 5 lists each component's pressure

ratings at the elevated temperatures, obtained using the temperature derating factors in Table 4. Recall that the maximum operating pressure is 1,000 psi. Note that the tubing, fittings, adapters, and top reservoir have pressure ratings well above 1,000 psi at approximately the maximum bulk oil temperature. The bottom reservoir, flow meter, and pump have lower temperature limits. These lower limits will nonetheless be met according to heat transfer approximations (found in Appendix D) due to the longer time and distance that the oil travels before it returns to these components. In addition, note that these components would only be subjected to high temperatures when the apparatus is operated in re-circulation mode.

Table 5 Test rig component pressure ratings at elevated temperatures.

Component(s)	Supplier	Rating at room temperature (psi)	Rating at high temperatures (psi)	
Valves, grafoil packing	hiP	20,000	20,000	at 800°F (427°C)
Valves, extended stuffing boxes	hiP	20,000	20,000	at 1,000°F (538°C)
Crosses, tees, tubing	hiP	20,000	15,700	at 850°F (454°C)
			15,400	at 1,000°F (538°C)
			7,400*	at 1,200°F (649°C)
Cone and thread to NPT adapters	hiP	15,000	11,775	at 850°F (454°C)
			11,550	at 1,000°F (538°C)
Bottom Reservoir	hiP	See Table 3.	1,700	at 950°F (510°C)
Top Reservoir	Hoke	5,000	3,850**	at 1,000°F (538°C)
			3,925**	at 850°F (454°C)
Flowmeter	Brooks Instruments	--	4,000	at 400°F (204°C)
Pump	Mahr Pump	--	4,270	at 665°F (350°C)

*Obtained using Parker's temperature de-rating factor for 316 stainless steel;
**Obtained using hiP's temperature derating factor for 316 stainless steel.

4. TESTING

4.1. Pressure Testing

Once the test rig was fully assembled and all connections were secured, a pneumatic test was performed to check for leaks and to ensure the pressure rating of the apparatus. The test performed was based on the ASME Boiler and Pressure Vessel Code [46]. According to the code, the pneumatic test pressure at every point in the system should be at least equal to 1.1 times the maximum allowable working pressure (MAWP) multiplied by the lowest stress ratio (LSR) for the material of which the vessel is constructed, shown in Equation (18). The stress ratio is the ratio of the stress value at its test temperature to the stress value at its design temperature [46].

$$PTP \geq 1.1 \times MAWP \times LSR = 1.1 \times MAWP \times \left(\frac{S_{test\ temperature}}{S_{design\ temperature}} \right) \quad (18)$$

Table 6 contains the maximum allowable stress, S, for 316 stainless steel according to the ASME code [47].

Table 6 Maximum allowable stress at various temperatures for 316 stainless steel.

Product form		Bar
Type/Grade		316
Maximum allowable stress (ksi)	-20 to 100°F	20.0
	1,000°F	15.3
	1,050°F	15.1
	1,200°F	7.4

Using 1,000 psi as the MAWP, 316 stainless steel as the material, room temperature as the test temperature and the maximum allowable stress values in Table 6, the pneumatic test pressures were calculated to be 1,446 psi for the entire system where the design temperature is 550°C (1,022°F) and 2,973 psi for the test section specifically where the design temperature is 650°C (1,200°F). The test pressures selected were therefore 1,500 psi and 3,000 psi for the entire system and the test section, respectively. Also, note that similar values are obtained when the inverse of the temperature derating factor at the design temperature is used instead of the LSR. This check agrees with the definition of both the temperature derating factor and LSR, and confirms the values provided by the manufacturers listed in Table 4.

The pneumatic tests were performed using nitrogen. The pressure was gradually increased to the test pressure, and the system and connections were inspected for leaks. All leaks found were corrected, and the test was performed again until the system held the test pressure for several minutes with no leaks detected. The performance of this test confirms that the system is rated for 1,000 psi when the temperature is at or below 650°C for the test section and 550°C for the remaining system components.

4.2. Oil Testing

To test the capabilities of the apparatus, a set of data was collected. The Standard Operating Procedure in Appendix A was followed during testing. Approximately 900 mL of SuperTech's conventional SAE 5W-30 motor oil was poured into the bottom reservoir for testing. The system was pressurized with nitrogen to 25 psig (39.61 psi), and it was manually maintained at this pressure during the test. The valves were set so that the flow

was in recirculation mode. The test section surface temperature was set to a maximum value of 595°C. The pump VFD was set to operate at 60 Hz, which corresponds to a flow rate of approximately 9.6 mL/min (~60 rpm × 0.16 mL/rev).

Temperature readings were taken and recorded every two seconds at the reservoir and test section inlet and outlet. The test section surface temperature is also of interest and would be recorded during normal testing, but it was not available for recording during this test. The test section temperature was measured, but the thermocouple was wired to the temperature controller which maintained the temperature to within 1°C from the set temperature.

Figure 22 shows the one-minute averages of the temperature traces recorded as well as the difference between the inlet and outlet oil temperature readings at a point in time, ΔT. A few important events that explain the shape of the curve are marked. Oil flow started at time $t = 0$ once the test section temperature reached 575°C, and a few minutes later the test section temperature was increased twice until it reached the final, maximum test section temperature of 595°C. This procedure resulted in the oil flowing over a test section surface that was between 575°C and 595°C for the first hour of recorded data. Soon after, a clear drop in outlet oil temperature of approximately 35°C was seen, and the oil temperatures remained constant for the remainder of the test, until the heaters and pump were turned off.

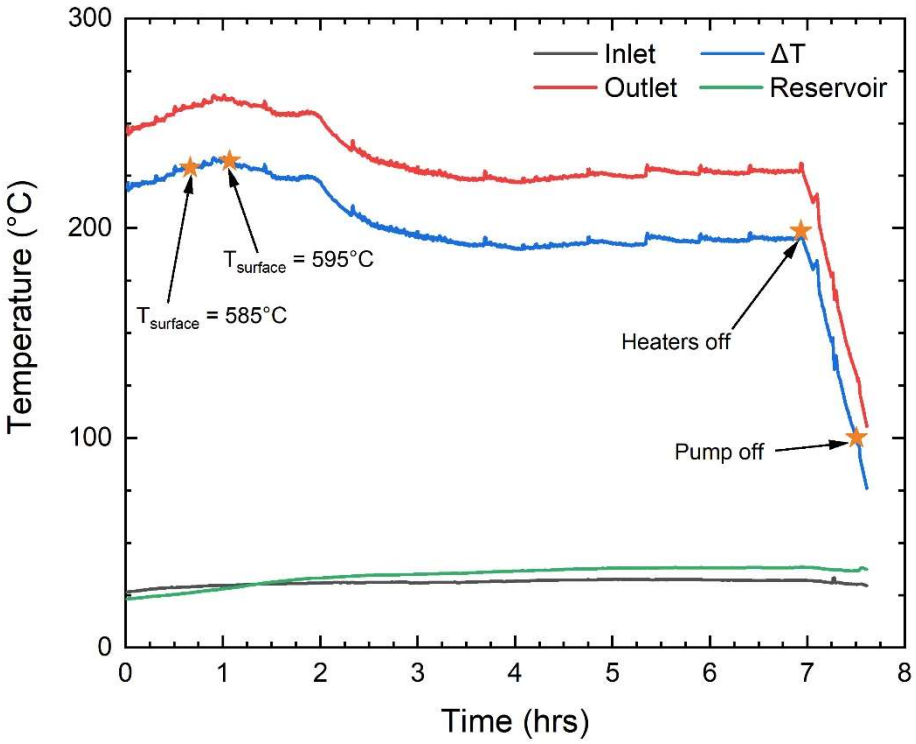

Figure 22 Temperature traces for SuperTech conventional motor oil SAE 5W - 30 with a surface temperature of 595 °C.

The system pressure increased with time due to the higher temperatures. The pressure was manually decreased to its original value (25 psig) approximately every half hour. The sudden peaks in the outlet temperature trace lasted only seconds and correspond to the times when the vent valve was opened, and nitrogen was quickly released.

Once the test ended, the test section was removed for analysis. Figure 23 shows the deposit buildup that formed. Note that the deposits were limited to the sections that were directly in contact with the heaters. The presence of the deposits confirms that the outlet temperature decrease was due to deposits building up and reducing the heat transfer to the flowing oil, as expected. The deposits were attached to the test section, were difficult

to remove, and had a grainy texture. They were slightly moist, perhaps because they were not allowed to dry; those that were removed a few days later were dry when removed.

(a)

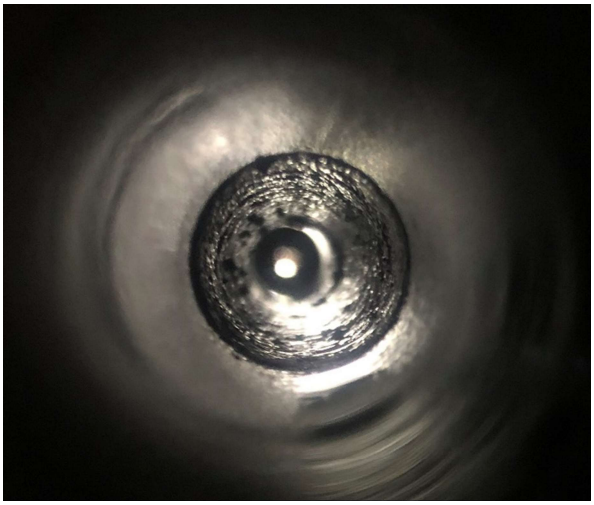

(b)

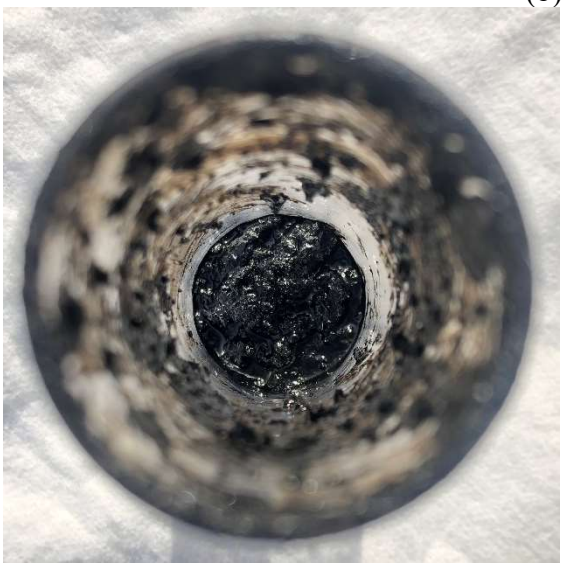

(c)

Figure 23 Deposits formed in test section for SuperTech conventional motor oil SAE 5W - 30 with a surface temperature of 595 °C. (a) and (b) show the deposits still in the test section tubing (c) shows the deposits collected after removal from the test section

In the initial testing process, other tests were run using a different oil, but no temperature decrease was seen. Figure 24 shows the temperature traces of one such test

using Mobil DTE 732 turbine oil, a test section surface temperature of 475°C, system pressure of 25 psig (39.7 psia), a VFD frequency of 60 Hz, 712 mL in the bottom reservoir, and the apparatus operating in recirculation mode. The traces show no decrease in ΔT, but rather a slight increase that can be explained by the rise in reservoir and inlet temperatures.

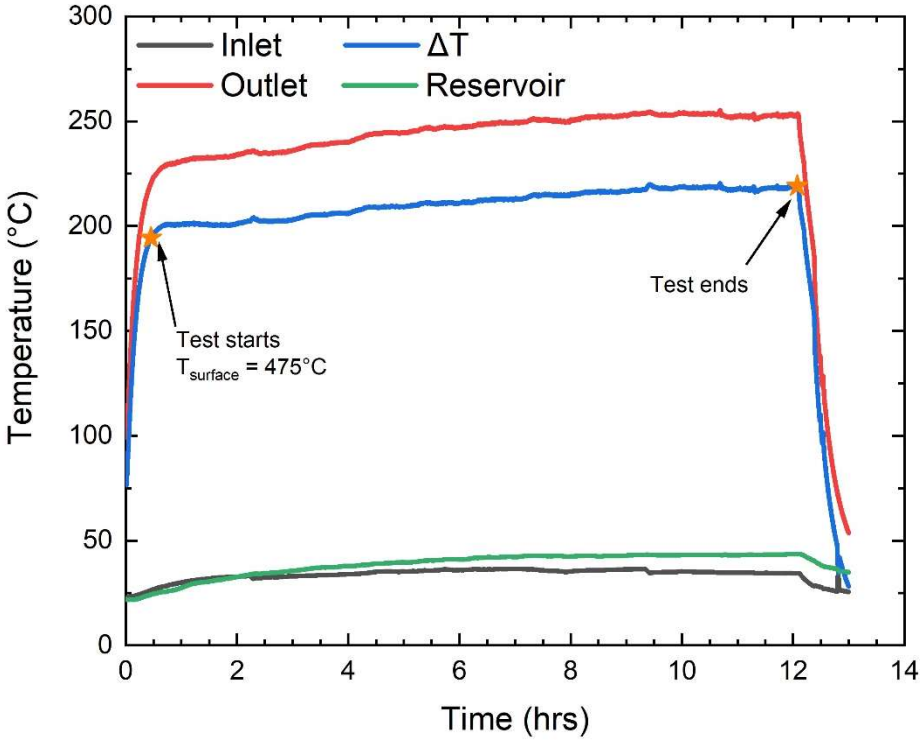

Figure 24 Temperature traces for Mobil DTE 732 turbine oil with a surface temperature of 475 °C.

The lack of deposit formation and decrease in ΔT may be because Mobil DTE 732 is a turbine oil and is therefore meant to withstand more-severe conditions than a conventional motor oil (like that shown in Figs. 22 and 23). Hence, to observe more-significant results, changes to the two main factors that affect the degradation process must be made, such as higher temperatures or longer test times, to allow the antioxidants to

deplete and the degradation process to begin. Note that the data shown in Fig. 22 and those in Fig. 24 cannot be directly compared since they were run at different surface temperatures, but Mobil DTE 732's resistance to degradation under the conditions of the test does indicate that such tests using the new facility in this thesis will reveal differences in various oils' performances.

5. CONCLUSIONS

5.1. Summary

A new test rig was developed and assembled as part of an effort to better understand the lubricating oil degradation process at high temperatures that leads to the formation of solid deposits. The experiment and apparatus take advantage of the importance that surface temperature, bulk oil temperature, and residence time have on the oil degradation process and of the insulation effect that deposit formation on hot surfaces has on the heat transfer between the hot surfaces and the lubricating oil that is meant to cool the system.

The apparatus is rated for a maximum test section temperature of 650°C and pressure of 1,000 psig. It consists of a flow loop with a heated test section through which the oil is pumped. It can operate in recirculation mode where the oil may pass through the heated test section several times, or in single-pass mode where the oil only encounters the high temperatures once. A small pump is used to generate the flow. The temperature and pressure of the oil before and after passing through the test section are measured.

During an experiment, the oil flows through a heated, constant-temperature test section which causes its temperature to rise. With time, as the deposits accumulate in the test section, the rise in oil temperature across the test section, ΔT, decreases. How fast this process occurs is an indicator of the oil's resistance to degradation. To test the apparatus, data were collected with SuperTech's conventional SAE 5W-30 motor oil and a maximum

test section surface temperature of 595°C. The test resulted in solid deposit formation over the heated surface and in a clear decrease in ΔT over the test period.

5.2. Future Work

As testing continues, a few changes may be made to the apparatus to improve its performance. First, the solid deposits that form during a test pose a risk to the pump's performance. Installing an oil filter either just after the test section or just before the pump would protect the pump against any damage from the deposits. Second, changing the test section geometry to one that has a higher ratio of heated surface area to oil mass flow rate may allow even higher bulk oil temperatures to be reached. An example of a possible geometry is an internal cylindrical heater contained within an outer tube, creating an annular cross section through which the oil flows.

The test rig is now capable of testing a wide variety of lubricating oils under many combinations of test surface temperatures, system pressures, and even test section geometries if so desired. Once several sets of data have been taken, the performance of different oils under the same test conditions may be compared and rated based on their induction time or amount of deposits formed.

REFERENCES

[1] Gschwender, L. J., Snyder, C. E., Nelson, L., Fultz, G. W., and Saba, C. S., 2001, Advanced High-Temperature Air Force Turbine Engine Oil Program Turbine Lubrication in the 21st Century, ASTM International, West Conshohocken, PA.
[2] Novotny-Farkas, F., Baumann, K., and Leimeter, T., 2008, "Optimizing the Thermo-Oxidation Stability of Gas Turbine Oils," Goriva I Maziva, 47(3), pp. 220 - 231.
[3] International, A., 2013, "ASTM Standard D4378: Standard Practice for In-Service Monitoring of Mineral Turbine Oils for Steam, Gas and Combined Cycle Turbines,"West Conshohocken, PA.
[4] ExxonMobil, 2016, "Tech Topic: Coking," E. Corporation, ed.
[5] Rudnick, L., 2009, Lubricant Additives Chemistry and Applications, Boca Raton: CRC Press.
[6] Kauffman, R., Feng, A., and Karasek, K., 2000, "Coke Formation from Aircraft Turbine Engine Oils: Part I — Deposit Analysis and Development of Laboratory Oil Coking Test," Tribology Transactions, 43(4), pp. 823 - 829.
[7] ASTM, 2014, "ASTM D2272: Standard Test Method for Oxidation Stability of Steam Turbine Oils by Rotating Pressure Vessel,"West Conshohocken, PA 19428-2959. United States.
[8] ASTM, 2018, "ASTMD943: Standard Test Method for Oxidation Characteristics of Inhibited Mineral Oils,"West Conshohocken, PA 19428-2959. United States.
[9] Pawlak, Z., 2003, Tribochemistry of Lubricating Oils Elsevier, Amsterdam.
[10] R. Mortier, M. Fox, and Orszulik, S. T., 2010, Chemistry and Technology of Lubricants, Springer.
[11] NoriaCorporation, 2012, "Base Oil Groups Explained," Machinery Lubrication.
[12] D. M. Pirro, M. Webster, and Daschner, E., 2016, Exxon Mobil: Lubrication Fundamentals, CRC Press.
[13] R. E. Kauffman, A. S. Feng, and Karasek, K. R., 2000, "Coke Formation from Aircraft Engine Oils: Part II - Effects of Oil Formulation and Surface Composition," Tribology Transactions, 43(4), pp. 677 - 680.
[14] Szydywar, J., 1984, "Ester Base Stocks," Journal of Synthetic Lubricants 1(2), pp. 153-169.
[15] Diaby, M., Sablier, M., Le Negrate, A., El Fassi, M., and Bocquet, J., 2009, "Understanding Carbonaceous Deposit Formation Resulting from Engine Oil Degradation," Carbon, 47(2), pp. 355-366.
[16] Mousavi, P., Wang, D., Grant, C., Oxenham, W., and Hauser, P., 2006, "Effects of Antioxidants on the Thermal Degradation of a Polyol Ester Lubricant Using GPC," Industrial & Engineering Chemistry Research, 45(1), pp. 15 - 22.
[17] Naidu, S., Klaus, E., and Duda, J., 1986, "Kinetic Model for High-Temperature Oxidation of Lubricants," Industrial & Engineering Chemistry Product Research and Development, 25(4), pp. 596 - 603.

[18] J. Fitch, and Gebarin, S., 2006, "Review of Degradation Mechanisms Leading to Sludge and Varnish in Modern Turbine Oil Formulations," Journal of ASTM International, 3(8).
[19] Miyata, I., Hirano, S., Tamada, M., and Fujimoto, K., 2015, "Mechanism of Turbocharger Coking in Gasoline Engines," SAE International.
[20] Grigor'ev, P., Tyurin, Y., Trusenev, M., and Vakhmyanina, M., 1977, "Resistance of Lubrication Oils to Coke Formation " Chemistry and Technology of Fuels and Oils, 13(11), pp. 815-817.
[21] Chernojookov, N., 1929, "Carbonization of Lubricating Oils and Fuel Oils," Industrial & Engineering Chemistry, 21(4), pp. 315-316.
[22] Yokoyama, F., and Iwama, Y., 2014, "Mechanism of Carbonaceous Deposit Formation Caused by Lubricating Oil on High Temperature Metal Surfaces," Tribology Online, 9(2), pp. 71-79.
[23] G. Livingstone, D. Wooton, and Thompson, B., 2007, "Finding the Root Causes of Oil Degradation," Practicing Oil Analysis.
[24] Schobert, H., 1990, The Chemistry of Hydrocarbon Fuels, Butterworth & Co.
[25] Chen, C., and Hsu, S., 2003, "A Chemical Kinetics Model to Predict Lubricant Performance in a Diesel Engine. Part I: Simulation Methodology," Tribology Letters, 4(2), pp. 83 - 90.
[26] Gatto, V., Moehle, W., Cobb, T., and Schneller, E., 2006, "Oxidation Fundamentals and Its Application to Turbine Oil Testing," Journal of ASTM International, 3(4).
[27] Zerla, F., and Moore, R., 1989, "Evaluation of Diesel Engine Lubricants by Micro-Oxidation," SAE Technical Paper Series(890239).
[28] Popovich, M., and Hering, C., 1959, Fuels and Lubricants, New York: John Wiley & Sons, Inc.
[29] Bakunin, V., and Parenago, O., 1992, "A Mechanism of Thermo-Oxidative Degradation of Polyol Ester Lubricants," Journal of Synthetic Lubrication, 9, pp. 127-143.
[30] 2011, "Aldol Reaction," Khan Academy.
[31] Clayden, J., Greeves, N., Warren, S., and Wothers, P., 2000, Organic Chemistry, Oxford.
[32] Severa, L., Havlíček, M., and Kumbár, V., 2009, "Temperature Dependent Kinematic Viscosity of Different Types of engine Oils," Acta Universitatis Agriculturae et Silviculturae Mendelianae Brunensis, 57(4), pp. 95 - 102
[33] Zuidema, H., 1945, "Oxidation of Lubricating Oils," Chemical Reviews, 38(2), pp. 197 - 226.
[34] Wiehe, I., 2008, Process Chemistry of Petroleum Macromolecules, Boca Raton: CRC Press.
[35] Prakoso, A., Punase, A., and Hascakir, B., 2017, "A Mechanistic Understanding of Asphaltenes Precipitation From Varying-Saturate-Concentration Perspectives," SPE Production & Operations, 32(01), pp. 086-098.
[36] Kagaya, M., and Ishikawa, S., 1984, "An Evaluation and Optimization of Lubricants for Turbocharged Gasoline Engines," SAE Technical Paper Series, 840261.

[37] Cazin, J., Abellaneda, G., Brégent, R., and Pascal, J., 1997, "Coking and Microcoking: Tools for Evaluating and Developing Lubricant Additives," Tribotest 4(2), pp. 167 - 179.
[38] Watkinson, A., 2003, "Comparison of Crude Oil Fouling Using Two Different Probes," Conference Proceedings of Heat Exchanger Fouling and Cleaning: Fundamentals and Applications.
[39] Branson, B., 2016, "Bench-Scale Testing for Rapid and Relevant Prediction of Crude Fouling Characteristics using the Hot Liquid Process Simulator," A. Petrolab, ed.San Antonio, TX.
[40] Srinivasan, M., and Watkinson, A., "Fouling of Some Canadian Crude Oils," Proc. Heat Exchanger Fouling and Cleaning: Fundamentals and Applications.
[41] Srinivasan, M., 2008, "Heat Exchanger Fouling of Some Canadian Crude Oils," Master of Applied Science, University of British Colombia.
[42] Company, H. P. E., 2020, "High Pressure Equipment Company Full Line Catalog."
[43] Baum, M. R., 1988, "Disruptive Failure of Pressure Vessels: Preliminary Design Guidelines for Fragment Velocity and the extent of Hazard Zone," Journal of Pressure Vessel Technology, 110.
[44] Hazell, P. J., 2015, Armour: Materials, Theory, and Design, CRC Press.
[45] Parker, 2009, "Instrument Tubing Selection Guide ".
[46] American Society of Mechanical Engineers, 2019, "ASME Boiler and Pressure Vessel Code: An International Code " Rules for Construction of Pressure Vessels Division 1.
[47] American Society of Mechanical Engineeers, 2015, "ASME Boiler & Pressure Vessel Code " Materials Part D Properties (Customary).
[48] F. P. Incropera, D. P. Dewitt, T. L. Bergman, and A. S. Lavine, 2011, Fundamentals of Heat and Mass Transfer, 7th ed. John Wiley & Sons.

APPENDIX A

STANDARD OPERATING PROCEDURE

Premises

1. The apparatus is fully assembled, and all connections are tightened.
2. Routine leak checks have been performed.
3. Pressure transducers and instrumentation are calibrated.
4. Test section tubing has been installed.

Procedure (reference Fig. A1 for valve numbering)

Beginning of experiment

1. Verify system status.
2. Verify the test section bypass line is closed (i.e. valves 3 and 5 are closed).
3. Open valve to vent (valve 9), and open valve above the bottom reservoir.
4. Insert the oil to be studied.
    a. Insert the oil into the bottom reservoir through the opened valve above it using a syringe.
    b. Close the valve above the bottom reservoir.
5. Pressurize the system.
    a. Open the gas bottle and regulator.
    b. Close vent valve.
    c. Open the valve that connects the bottle to the apparatus (valve 10) and allow pressure to rise above atmosphere. Close valve 10.

d. Open vent valve to release gas but keep pressure above atmosphere (~14.7 psi).

e. Repeat steps b, c, and d.

f. Open valve 10 and fill to desired system pressure (upper limit of 1000 psia).

g. Close valve 10.

6. Set the route the oil is to follow. If in re-circulation mode, open valve 7 and close valve 6. If in single-pass mode, open valve 6 and close valve 7.
7. Place the "High Surface Temperature" warning sign.
8. Turn temperature controller/test section heater on.
9. Increase set temperature gradually until desired test temperature is reached.
10. Set desired pump settings using the pump VFD/inverter. The chosen pump speed will determine the flow rate.
11. Turn pump on. Allow oil to start flowing.
12. Confirm the flowrate using the flowmeter.
13. Allow the test section surface temperature to return to its set value.
14. Start the data acquisition process.

Ending of experiment

1. Turn off heater.
2. Allow test section surface temperature to lower below 200°C.
3. Turn off pump.
4. De-pressurize the system by opening the vent valve.

5. Drain the oil from the apparatus by opening the valves below the bottom and/or top reservoirs.
6. Remove test section tubing for further analysis.

Cleaning of apparatus and preparing for next experiment

1. Check system status. System must be at atmospheric pressure with heater off.
2. Fill the bottom reservoir with an oil solvent or paint thinner.
3. Turn pump on and allow the solvent to circulate for a few minutes.
4. Drain the top and bottom reservoirs.
5. Allow remaining solvent to evaporate.
6. To prepare for the next run, repeat steps one through four with the new oil to be tested instead of an oil solvent.

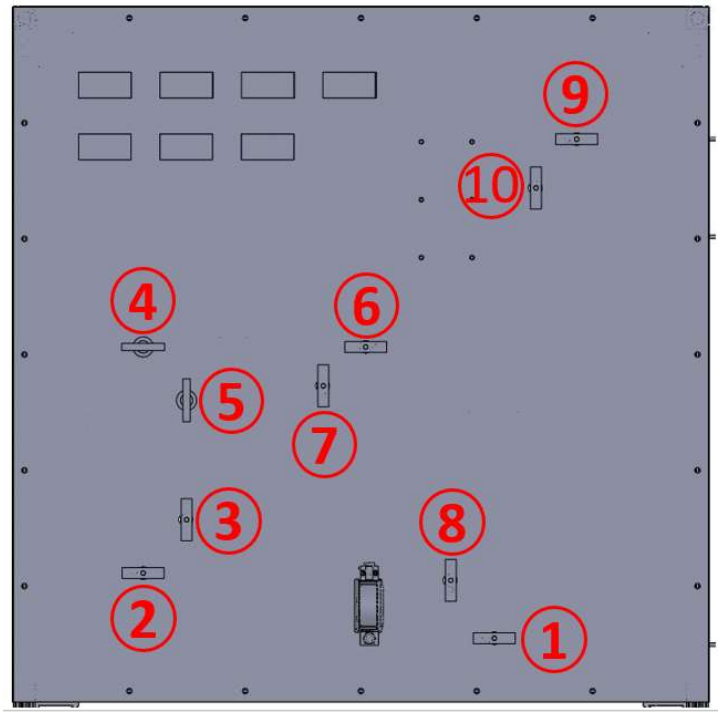

Figure A1 Valve labeling for the Standard Operating Procedure.

APPENDIX B

LIST OF SOME OF THE ITEMS USED FOR TEST RIG ASSEMBLY

Table B1 Items used in the test rig supplied by the High Pressure Equipment Company.

Item Name	**Product Code**	**Quantity**
Valves (with High Temperature Extension)	20-11LF4-HT	2
Valves (normal)	20-11LF4	11
Ball check valve.	20-41LF4	1
Cross	20-24LF4	2
Tees	20-23LF4	13
Adaptor, 1/4” M.P. Female to 1/4” NPT Male	20-21LF4NMB	2
Adaptor, 1/4” M.P. Male to 1/4” NPT Female	20-21NFBLM4	1
Adaptor, 1/4” M.P. Female to 1/2” NPT Male	20-21LF4NMD	2
Adaptor, 1/4" M.P. Female to 1" M.P. Female	20-21LF4LF16	2
Gland, 1/4" Tubing	20-2LM4	2
Plug, 1/4" Tubing	20-7LM4	3
Series BC Reactors	BC-2	1
Tubing, 1/4" O.D. x 0.109" I.D. (M.P. LF4)	20-9M4-316	--
Tubing, 1" O.D. x 0.562" I.D. (M.P. LF16)	20-9M16-316	--

Table B2 Items used in the test rig supplied by Omega Engineering.

Item name	Product Code	Quantity
Dual Rugged Heavy-Duty Transition Joint Thermocouple Probes	TJ36-CAIN-18U-6-DUAL	1
Dual Element Thermocouple Assemblies with Miniature Size Connector	SCASS-062U-3-DUAL	2
Dual Element Thermocouple probe with Standard Size Connector	CASS-116G-12-DUAL	1
Rugged Heavy-Duty Transition Joint Thermocouple Probes	TJ36-CAIN-18U-3-CC	1
Cooling Element	PG-CTN4-G03	1
High Watt Density Band Heaters	MPP50301	2
PLATINUM™ Series Digital Panel Meters	DP8PT	7
High Accuracy Oil Filled Pressure Transducers/Transmitters for General industrial applications	PX409-1.5KGV	1

Table B3 Items used in the test rig supplied by various manufacturers.

Item	Company	Product Code	Qty
Formed Sampling Cylinders	AWC/Hoke	HO 8HPDY1000	1
Pump, "MarSpin" Gear Metering Pump	Mahr	--	1
MK200 Series Melt Pressure Transducers	MPI Morheat	MK201P1.5MSI-.25%	2
6 pin Bayonet cable for MK200 transducer	MPI Morheat	MP-CAB-6B-PN12	2
Thermocouple and Voltage DAQ and Data Logger System	DATAQ	DI-2008	1

APPENDIX C

MELT PRESSURE TRANSDUCER ADAPTOR FEA ANALYSIS RESULTS

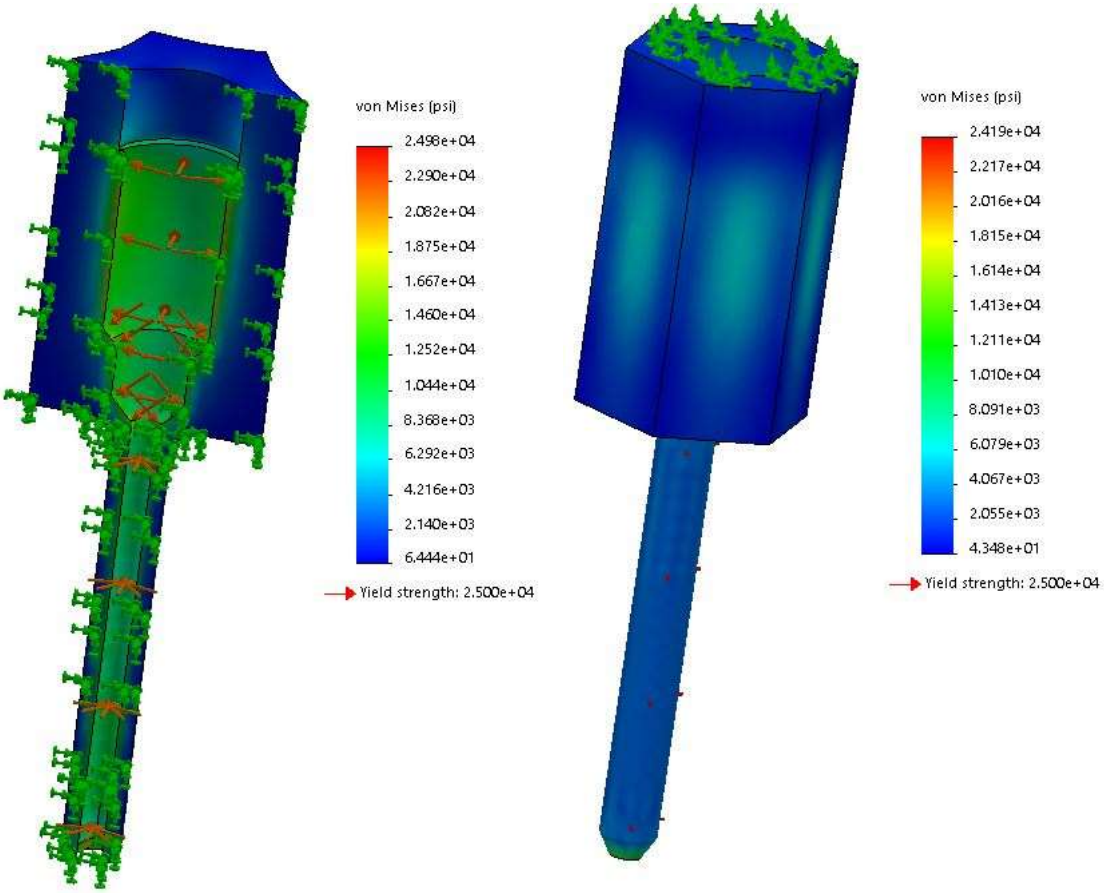

(a) (b)

Figure C1 MPI pressure adaptor FEA analysis results when a pressure of 6,685 psi is applied (a) due to symmetry, only half of the model was meshed; symmetry determined the boundary conditions; (b) the entire adaptor was meshed.

APPENDIX D

HEAT TRANSFER ANALYSIS

Cooling of oil

T_∞:	Outside air temperature	$T_{s,i}$:	Inner surface temperature
T_1:	Initial oil temperature	$T_{s,o}$:	Outer surface temperature
T_2:	Final oil temperature	A_s:	Tube surface temperature

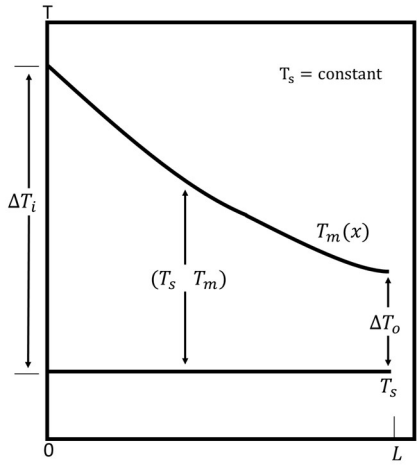

Figure D1 Axial temperature variations for heat transfer in a tube, constant temperature of external fluid [48].

The following steps and equations were used to obtain an approximation of the tubing length necessary to cool the oil from T_1 to T_2.

To calculate the inner convection heat transfer coefficient (fluid: engine oil at 430K):

$$Re_D = \frac{\rho \bar{V} D}{\mu} = \frac{\bar{V} D}{\nu} \qquad \text{Step 1}$$

Check if fully developed $\left(\frac{x_{fd,h}}{D}\right)_{lam} \approx 0.05 Re_D$ Step 2

Laminar, fully developed flow, uniform T_s	$Nu = 3.66$	Step 3
	$h_i = \frac{k \cdot Nu}{D_h}$	Step 4

To calculate the outer convection heat transfer coefficient (fluid: air at 560K):

Guess $T_{s,o}$	$Ra_L = \frac{g\beta(T_{s,o} - T_\infty){L_{char}}^3}{\nu\alpha}$	Step 5
Long, horizontal cylinder for $Ra_D \leq 10^{12}$	$\overline{Nu_D} = \left\{0.60 + \frac{0.387Ra_D^{1/6}}{[1 + (0.559/Pr)^{9/16}]^{8/27}}\right\}^2$	Step 6
	$h_o = \frac{\overline{Nu_D}k}{D_o}$	Step 7

To calculate the outer surface temperature (fluid: air at 560K):

	$(L \cdot R_{tot}) = \frac{1}{h_i \cdot 2\pi r_i} + \frac{\ln(r_o/r_i)}{2\pi k_{ss}} + \frac{1}{h_o \cdot 2\pi r_o}$	Step 8
Only really true at test section exit	$\frac{q}{L} = \frac{T_1 - T_\infty}{(L \cdot R_{tot})}$	Step 9
	$T_{s,o,calc} = T_1 - \left(\frac{q}{L}\right)\left(\frac{1}{h_i \cdot 2\pi r_i} + \frac{\ln(r_o/r_i)}{2\pi k_{ss}}\right)$	Step 10
Iterate until	$T_{s,o,guess} - T_{s,o,calc} = 0$	Step 11

To calculate length of tubing to achieve required temperature decrease (fluid: air at 510K):

	$Ra_L = \frac{g\beta(T_{s,o,calc} - T_\infty){L_{char}}^3}{\nu\alpha}$	Step 12

Long, horizontal cylinder for $Ra_D \leq 10^{12}$	$\overline{Nu_D} = \left\{0.60 + \frac{0.387Ra_D^{1/6}}{[1+(0.559/Pr)^{9/16}]^{8/27}}\right\}^2$	Step 13
	$h_o = \frac{\overline{Nu_D}k}{D_o}$	Step 14
	$\overline{U} = \frac{1}{R_{tot}A_s}$	Step 15
	$R_{tot} = \frac{1}{h_i \cdot 2\pi r_i L} + \frac{\ln(r_o/r_i)}{2\pi kL} + \frac{1}{h_o \cdot 2\pi r_o L}$	
Let $A_s = 2\pi r_i L$	$\frac{1}{\overline{U}} = R_{tot}A_s = \frac{1}{h_i} + \left(\frac{r_i}{k}\right)\ln(r_o/r_i) + \left(\frac{r_i}{r_o}\right)\frac{1}{h_o}$	
	$\frac{\Delta T_o}{\Delta T_i} = \frac{T_\infty - T_2}{T_\infty - T_1} = exp\left(-\frac{\overline{U}A_s}{mC_P}\right)$	Step 16
	$L = \frac{-\ln(\Delta T_o/\Delta T_i)mC_P}{\overline{U} \times \pi D}$	

The Table D1 summarize the fluid and material properties used when calculating the values above, and Table D2 provides a summary of the results.

Table D1 Fluid properties used in heat transfer calculations [46].

Fluid	Engine Oil	Air		Stainless Steel
Temperature (K)	**430**	**510**	**560**	**500**
k (W/m·K)	0.132	0.04134	0.0445	16.75
ν (m^2/s)	5.83E-06	4.01E-05	4.7E-05	--
β (K^{-1})	0.0007	0.0033	0.0033	--
α (m^2/s)	6.2E-08	5.87E-05	6.87E-05	--
Pr	88	0.6838	0.6834	--
ρ (kg/m^3)	806.5	0.6837	0.6224	--
Cp (kJ/kg·K)	2.471	1.032	1.0422	--

Table D2 Length of tubing required for oil to cool down from T_1 = 550°C to T_2 at various flow rates.

Q (mL/min)		5	10	15	20
T_2 (°F)	**T_2 (°C)**	**Length (in)**			
1000	538	0.512	1.025	1.537	2.050
950	510	1.756	3.513	5.269	7.025
850	454	4.475	8.951	13.426	17.901
750	399	7.516	15.032	22.548	30.064
650	343	11.111	22.221	33.332	44.443
550	288	15.319	30.638	45.957	61.276
450	232	20.625	41.251	61.876	82.502
400	204	23.8846	47.692	71.539	95.385

APPENDIX E

PART DRAWINGS

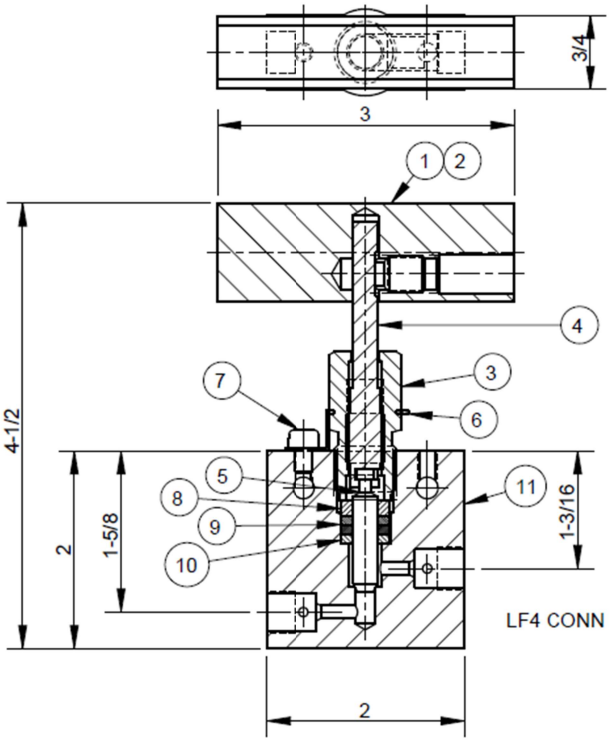

BILL OF MATERIAL				
ITEM	QTY	DESCRIPTION	PART NO.	MATERIAL
1	1	SOC SET SCREW	B01489	STEEL
2	1	HANDLE	212435	ALUMINUM
3	1	PACKING GLAND	213935	AMPCO_45
4	1	UPPER STEM	213934	17-4_PH_H1150
5	1	LOWER STEM	213933	17-4_PH_H900
6	1	LOCKING DEVICE	207733	316
7	1	10-32 X 1/4 FILL HD SCR	B01390	316
8	1	TOP PACKING WASHER	207731	316
9	2	PACKING	B01392	TEFLON
10	1	BOTTOM WASHER	207732	316
11	1	VALVE BODY	207739	316
12	2	COLLAR	20-2L4	316
13	2	GLAND	20-2LM4	316

20-11LF4
316SS
20000 PSI

NO.	REVISION	DATE	BY
0	DCN 16-0074	08/16/16	DF

HIGH PRESSURE EQUIPMENT COMPANY
ERIE, PENNSYLVANIA USA

		404819
DF	2015/12/07	

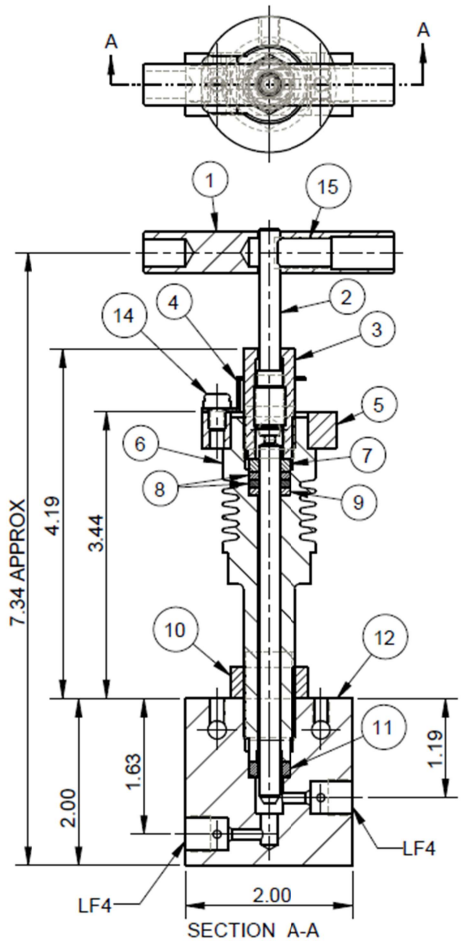

SECTION A-A
SCALE 0.850

BILL OF MATERIAL

ITEM	QTY	DESCRIPTION	PART NO.	DRAWING NO.	MATERIAL
1	1	HANDLE	200151	200151	ALUMINUM
2	1	STEM ASSEMBLY	208262	208262	17-4PH
3	1	PACKING GLAND	207730	207730	316SS
4	1	LOCKING DEVICE	207733	207733	300 SER. SS
5	1	LOCKING DEVICE ADAPTER	208263	208263	300 SER. SS
6	1	HOUSING	208264	208264	316SS
7	1	TOP PACKING WASHER	207731	207731	316SS
8	2	PACKING	B01391		GRAFOIL
9	1	BOTTOM PACKING WASHER	207732	207732	316SS
10	1	5/8-18 JAM NUT	B01505		300 SER. SS
11	1	SEAL RING	208265	208265	316SS
12	1	BODY	207739	207739	316SS
14	1	10-32 X 1/4 FILL HD SCR.	B01390		300 SER. SS
15	1	SOC SET SCREW	B01489		STEEL
16	2	COLLAR	20-2L4	207721	316SS
17	2	GLAND	20-2LM4	207724	316SS

NO.	REVISION	DATE	BY
1	REARRANGED TABLE INFORMATION	04/19/01	DF

DIMENSIONS IN INCHES

HIGH PRESSURE EQUIPMENT COMPANY
ERIE, PENNSYLVANIA USA

VALVE ASSEMBLY
1/4 MEDIUM PRESSURE 20-11LF4-HT

APPVD DF | ORDER | DATE 04/18/01 | DRAWING NO. 403164

DESIGN PRESSURE 5000 PSI AT 650 °F
HYDROSTATIC TEST PRESSURE 8,000 PSI
APPROXIMATE CAP SCREW TORQUE 75 FT LBS
APPROXIMATE ASSEMBLY WEIGHT 55 LBS
APPROXIMATE COVER WEIGHT 12 LBS

BILL OF MATERIALS

ITEM	QTY	DESCRIPTION	PART NO.	MATERIAL
1	8	7/8-9 SCREW	B01432	SA-193_B7
2	1	COVER	604253	316
3	1	GASKET	206849	316
4	1	BODY	604252	316
5	1	GASKET	B00301	COPPER
6	1	THERMOWELL	201523P21	316
7	3	COLLAR	20-2L4-SP1	316
8	3	GLAND	20-2LM4	316
9	1	3/8-16 EYE BOLT (NOT SHOWN)	B00601	STEEL

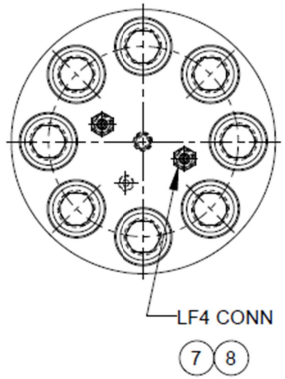

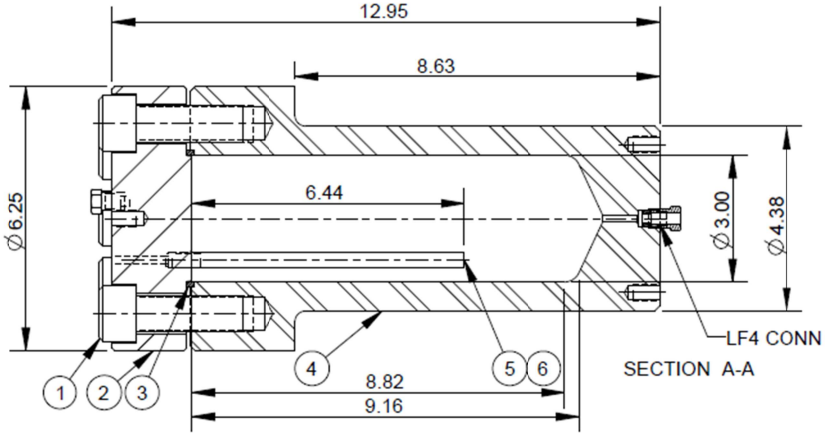

SECTION A-A

STANDARD TOLERANCES AND MANUFACTURING PRACTICES SPECIFICATION ES-002 APPLIES TO THIS DRAWING		STANDARD TOLERANCES	
		X.XXX± 0.005	
		X.XX± 0.01	
		FRACTIONAL ± 1/64	
0	SR 20-0242	2020-07-28	JY
REV	REVISION	DATE	BY

HIGH PRESSURE EQUIPMENT A GRACO CO
ERIE PENNSYLVANIA USA

BC-2 REACTOR

SHEET 1 OF 1

DRAWN BY JY 2020-07-29

604251

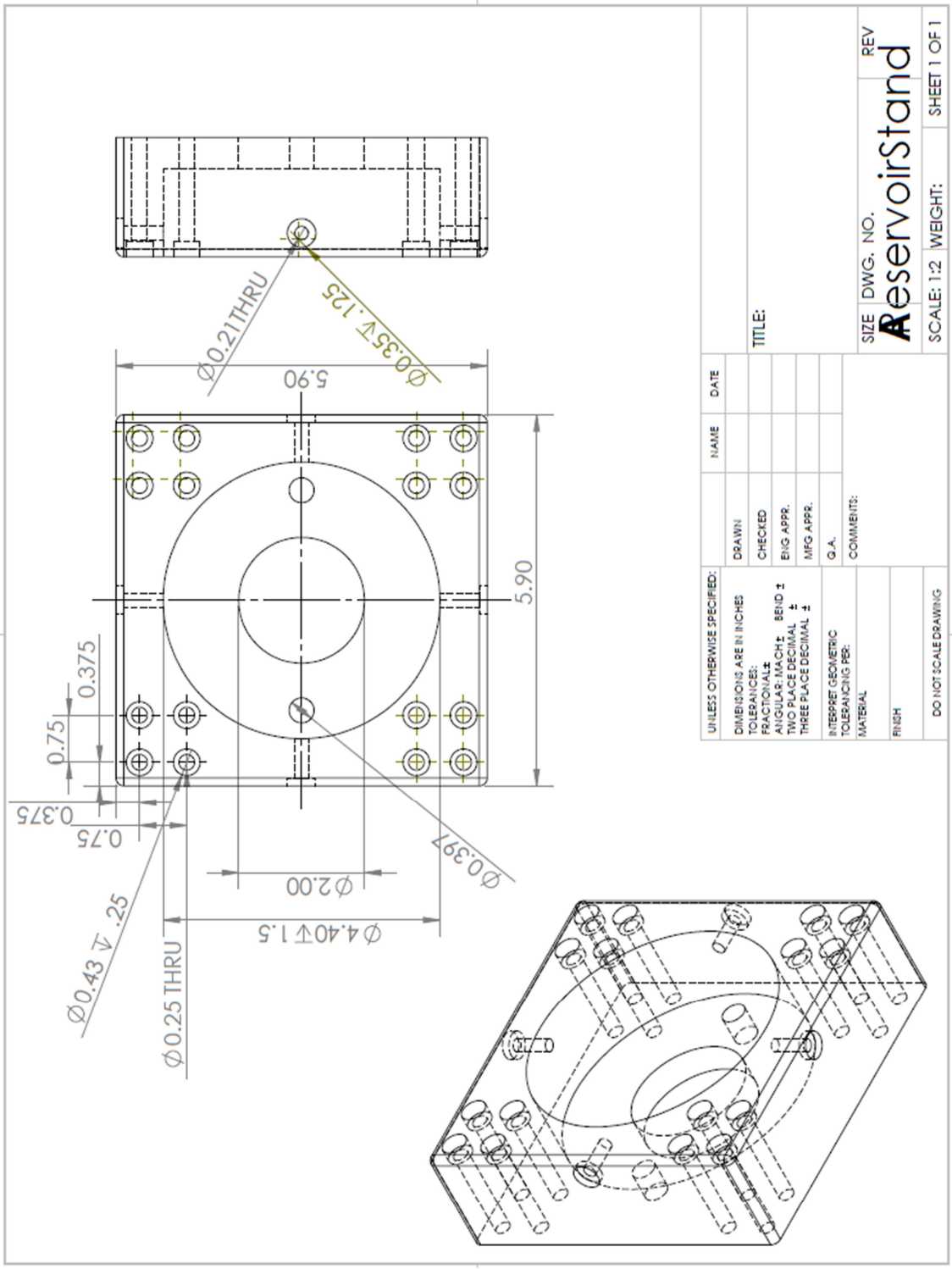
Ø0.21THRU
Ø0.35↧1.25
5.90
5.90
0.375
0.75
0.375
0.75
Ø0.397
Ø2.00
Ø4.40↧1.5
Ø0.43 ⊽ .25
Ø0.25 THRU
UNLESS OTHERWISE SPECIFIED:
DIMENSIONS ARE IN INCHES
TOLERANCES:
FRACTIONAL±
ANGULAR: MACH± BEND ±
TWO PLACE DECIMAL ±
THREE PLACE DECIMAL ±
INTERPRET GEOMETRIC TOLERANCING PER:
MATERIAL
FINISH
DO NOT SCALE DRAWING
NAME
DATE
DRAWN
CHECKED
ENG APPR.
MFG APPR.
Q.A.
COMMENTS:
TITLE:
SIZE
DWG. NO.
REV
ReservoirStand
SCALE: 1:2
WEIGHT:
SHEET 1 OF 1

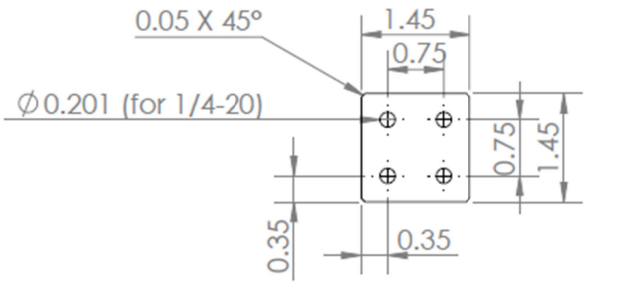

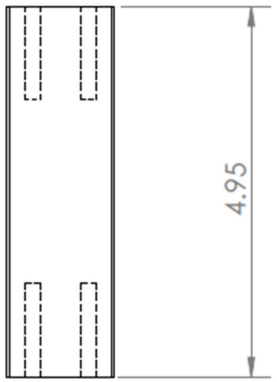

		UNLESS OTHERWISE SPECIFIED:		NAME	DATE
		DIMENSIONS ARE IN INCHES TOLERANCES: FRACTIONAL ± ANGULAR: MACH ± BEND ± TWO PLACE DECIMAL ± THREE PLACE DECIMAL ±	DRAWN		
			CHECKED		
			ENG APPR.		
			MFG APPR.		
		INTERPRET GEOMETRIC TOLERANCING PER:	Q.A.		
		MATERIAL	COMMENTS:		
NEXT ASSY	USED ON	FINISH			
APPLICATION		DO NOT SCALE DRAWING			

TITLE:

SIZE	DWG. NO.	REV
A	Legs	
SCALE: 1:2	WEIGHT:	SHEET 1 OF 1

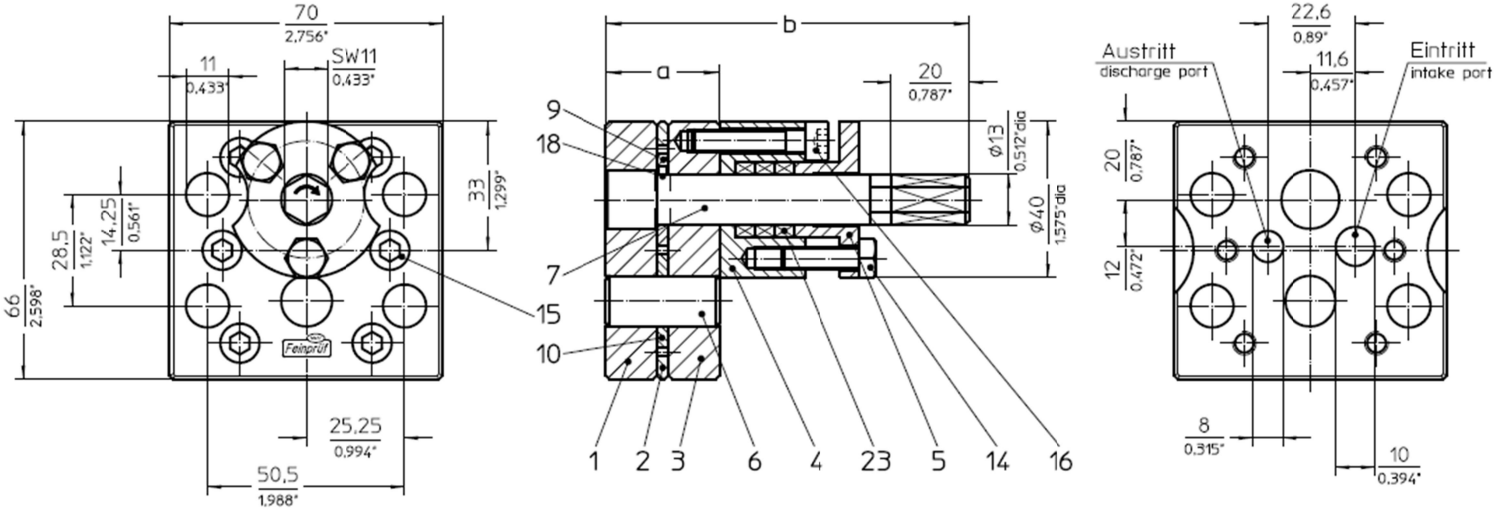

Typ type	a		b	
	mm	inch	mm	inch
0,16	28	1,102"	92	3,622"
0,2	28,5	1,122"	92,5	3,642"
0,25	29	1,142"	93	3,661"

Bei Ersatzteil-Bestellung bitte angeben:
1. Zeichnungs-Nummer
2. Typ
3. Teil-Nummer
4. lfd. Nummer der Pumpe
5. Material

when ordering spare parts please specify:
1. drawing number
2. type
3. number of the part
4. number of the pump
5. material

Stück piece	Teil part	Benennung	denomination
3 (5)	23	Stopfbuchspackungsring	packing ring
1	18	Zylinderstift	cylindrical pin
3	16	Zylinderschraube M6	cylindrical screw M6
6	15	Zylinderschraube M6	cylindrical screw M6
3	14	Sechskantschraube M6	hexagon screw M6
1	10	Zahnrad ohne Nut	driven metering gear
1	9	Zahnrad mit Nut	driving metering gear
1	7	Antriebswelle	driving arbor
1	6	Lagerachse	stud
1	5	Preßflansch	stuffing pressure flange
1	4	Dichtungsgehäuse	seal chamber
1	3	Oberplatte	hub plate
1	2	Gehäuse	center plate
1	1	Unterplatte	back plate

Index	Änderung	Änd.-Nr.	verifiziert	Datum	Name

Benennung: Einfach Spinnpumpe Typ 0,16-0,25 cm³/U

denomination: spinning pump (1-stream) type 0,16-0,25 cc/rev.

Ident-Nr.

Material

Allgemeintol. DIN ISO 2768-k (generaltolerances)

bis 6	± 0,1
über 6 – 30	± 0,2
über 30 – 120	± 0,3
über 120 – 400	± 0,5
über 400 – 1000	± 0,8
über 1000	± 1,2

Zeichnungs-Nr. S1-0,16-0,25/4D3AZ Blatt /

Ersatz Zeichnung gleicher Nr. vom 19.05.76

	Datum	Name
gezeichnet	09.09.92	hoffmann
geprüft		

Mahr

Mahr Metering Systems GmbH
Brauweg 38
D-37073 Goettingen / Germany

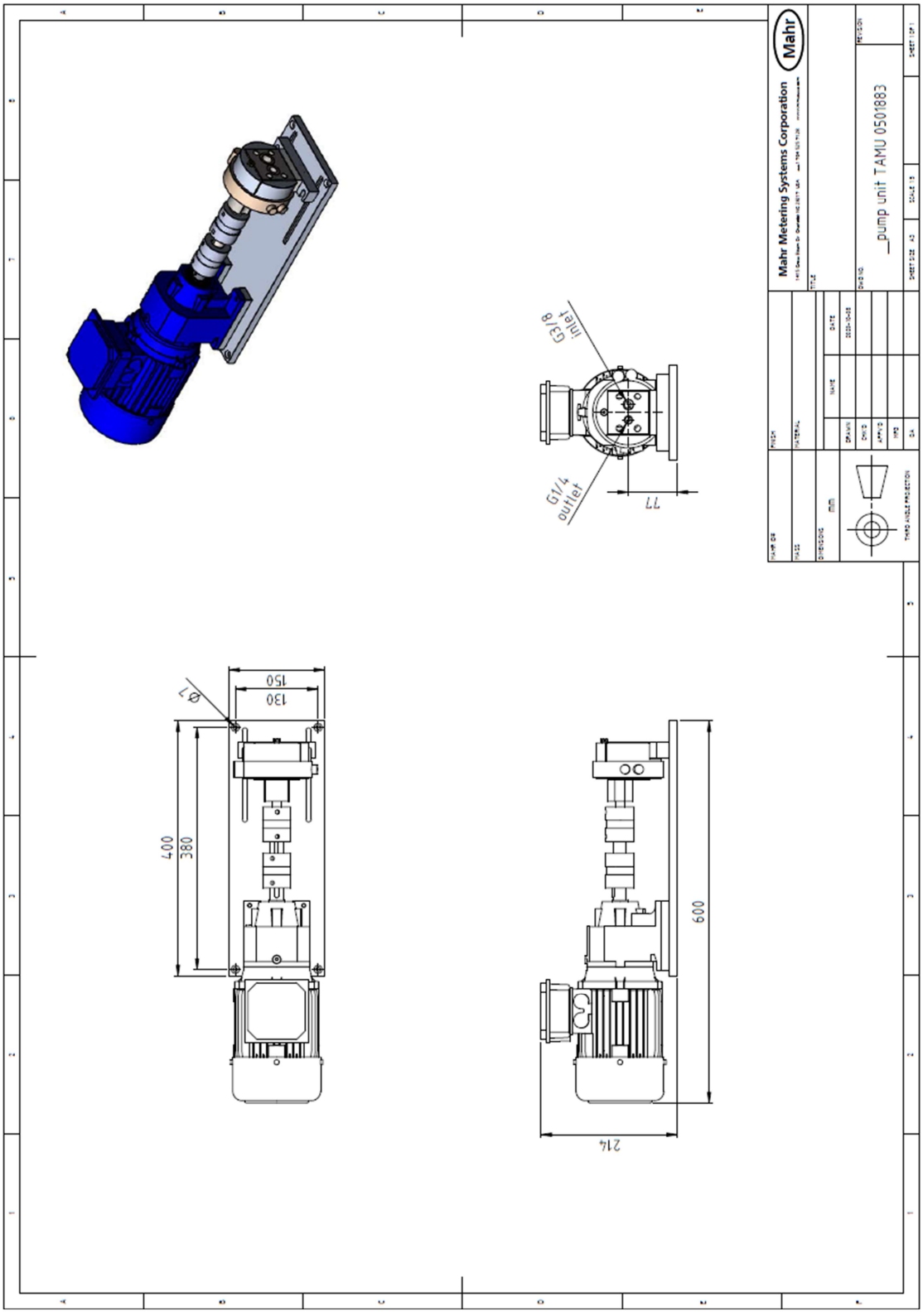
Mahr Metering Systems Corporation
Mahr
_pump unit TAMU 0501883
G3/8 inlet
G1/4 outlet
77
150
130
Ø7
400
380
600
214

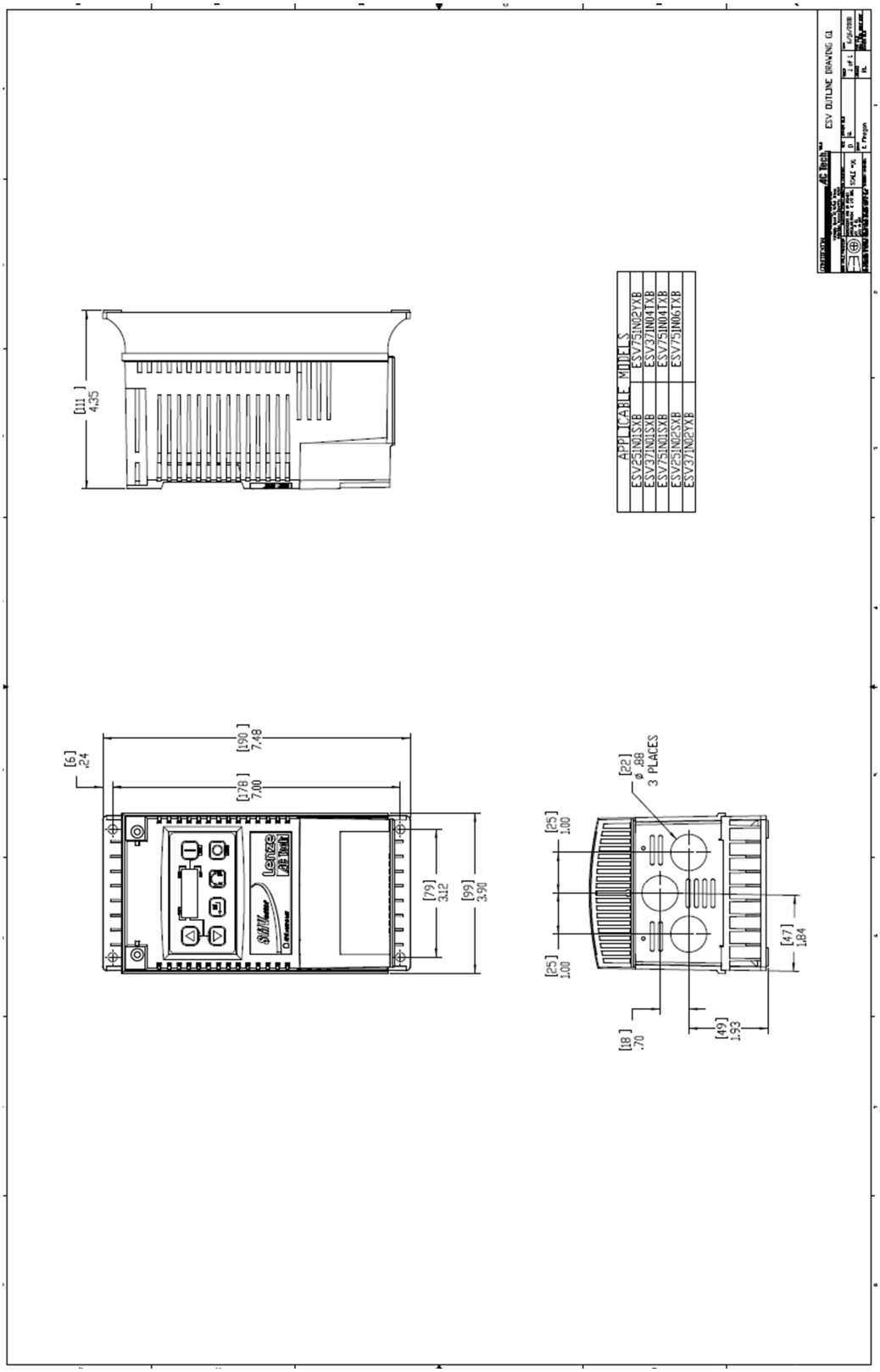
ESV OUTLINE DRAWING 01
APPLICABLE MODELS
ESV251N01SXB
ESV371N01SXB
ESV751N01SXB
ESV251N02SXB
ESV371N02YXB
ESV751N02YXB
ESV371N04TXB
ESV751N04TXB
ESV751N06TXB
[111] 4.35
[6] .24
[190] 7.48
[178] 7.00
[79] 3.12
[99] 3.90
[22] ø .88 3 PLACES
[25] 1.00
[25] 1.00
[47] 1.84
[18] .70
[49] 1.93

CAD DRAWING - NO MANUAL REVISIONS ALLOWED | 3 | 2 | DWG NO. 8HPDY SER. | SHT 1

3/16 HIGH CHARACTERS ON CYLINDER WITH 1000CC CAPACITY
1/8 HIGH CHARACTERS ON CYLINDER LESS THAN 1000CC CAPACITY

REVISIONS			
REV	DESCRIPTION	DATE	APPROVED
F	SEE PERMANENT RECORD		
G	SEE ECO 13561C	00/01/25	HH
H	SEE ECO 14806C	00/11/08	AHL
J	SEE ECO 15753C	01/06/20	AHL
K	SEE ECO 16424C	01/10/22	AHL
L	SEE ECO 19144C	03/5/29	M. Eb.

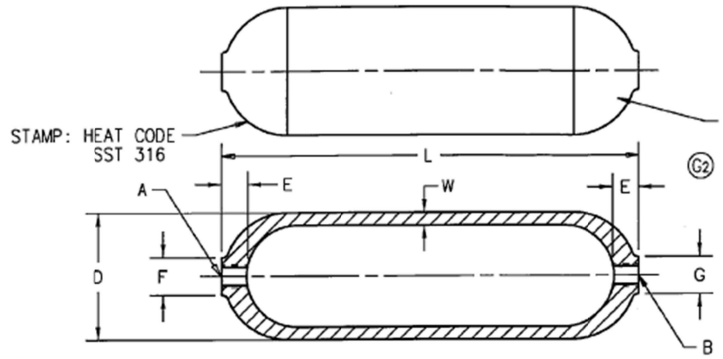

(J)
STAMP AS FOLLOWS:
DOT-3A 5000 HOKE [ ]-[ ] ← TEST DATE MONTH & YEAR
(G2) [ ] [ ] A [ ] 316 SST ← YEAR & SERIAL NUMBER
INSPECTOR'S STAMP

(J)

PART NO.	TUBE CUT-OFF LENGTH +1/16 -0	A NPT	B NPT	E	F MIN.	G MIN.	L1	D	W	MATERIAL CODE No.	APPROX WEIGHT LBS
8HPDY300	13	1/2	1/2	5/8	1 1/8	1 1/8	12 1/2 ±1/8	2.000 +.016 -.031	.250 +.055 -.000	714CT1874	5
8HPDY500	20	1/2	1/2	5/8	1 1/8	1 1/8	19 1/2 ±1/8	2.000 +.016 -.031	.250 +.055 -.000	714CT1874	8
(K) 8HPDY1000	15	1/2	1/2	5/8	1 1/8	1 1/8	14 3/4 ±1/4	3.500 ±.031	.437 +.066 -.055	714CT1781	17 1/2
(L) 8HPDY1100-SHORT	11 3/4	1/2	1/2	5/8	1 1/8	1 1/8	11 ±1/4	4.500 ±.031	.531 +.080 -.066	196CT1934	23
8HPDY2250	18 1/2	1/2	1/2	5/8	1 1/8	1 1/8	18 ±1/4	4.500 ±.031	.531 +.080 -.066	196CT1934	35
(J) 8HPDY3000	26	1/2	1/2	5/8	1 1/8	1 1/8	24 3/4 ±1/4	4.500 ±.031	.531 +.080 -.066	196CT1934	45
8HPDY1G	28 3/4	1/2	1/2	5/8	1 1/8	1 1/8	28 1/4 ±1/4	4.500 ±.031	.531 +.080 -.066	196CT1934	55
8HPDY2 1/2G	32 1/4	1/2	1/2	5/8	1 1/8	1 1/8	31 3/4 ±1/2	6.625 +.062 -.031	.719 +.108 -.090	712CT1944	124

NOTES:
1. 8HPDY300 & 500 HOT FINISHED SEAMLESS 316 SST TUBING TO ASTM A511; 8HPDY1000 AND LARGER HOT FINISHED SEAMLESS 316 SST PIPE TO ASTM A312.
2. VOLUME TOLERANCE: +20%, -0%
3. STAMP ALL DOT DATA AS SHOWN.
4. NORMALIZE IN 200°F WATER FOR 30 MINUTES.
(G1) 5. AFTER NORMALIZATION, HYDROSTATIC TEST AT 8350 PSIG.
6. FOR NACE APPLICATIONS, SPECIAL HEAT TREATMENT IS REQUIRED.
(J) 7. FOR CYLINDERS REQUIRING UK H&SE CERTIFICATION, SEE DRAWING 8HPDY-HSE.

RATED PRESSURE: 5000 PSI

UNLESS OTHERWISE SPECIFIED:
DIMENSIONS IN INCHES
REMOVE BURRS
FILLET RADII .005 TO .035
MACHINE FINISH 125
DRILL POINTS 5/16
TOLERANCES ARE:
DECIMALS: .XX = ±.010
.XXX = ±.005
ANGLES: ±1°
CONCENTRICITY .010 DIA
DO NOT SCALE DRAWING

APPROVALS		DATE
DRAWN	DJT	94/06/15
CHECKED	WR	95/06/16
APPROVED	PZ	95/06/16

INITIAL USAGE (REF ONLY)
CAD FILE: 8HPDY

SEE NOTE 1	-	
MATERIAL	FINISH	ITEM NO.

HOKE INC

TITLE: STANDARD HIGH PRESSURE CYLINDER 1/2 NPT, DOT-3A 5000

SIZE	CAGE CODE	DWG NO.	REV
B	28968	8HPDY SER.	L

SCALE NONE | DATE: MT | ACT. MT | SHEET 1 OF 1

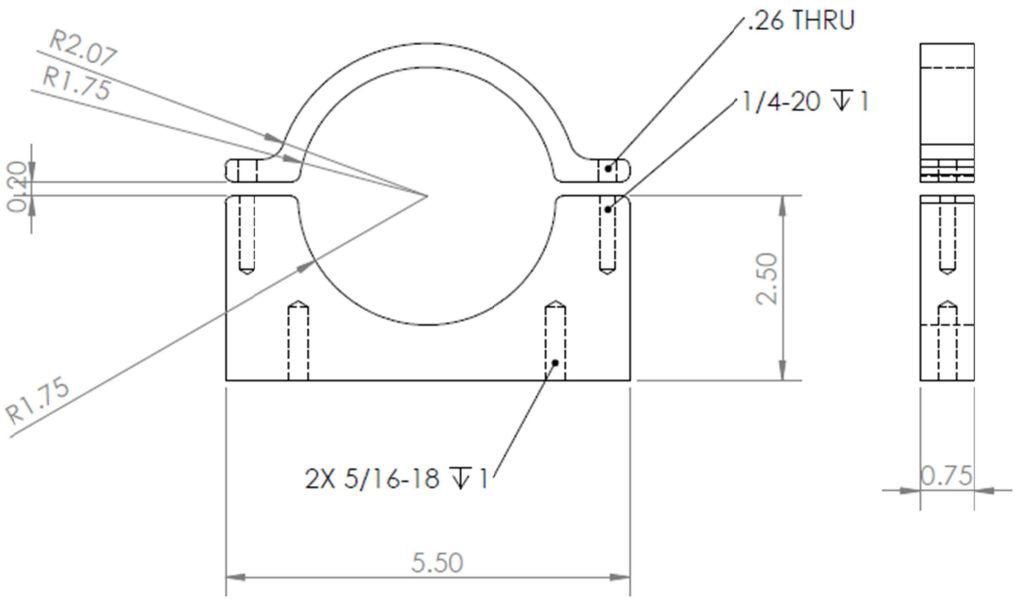

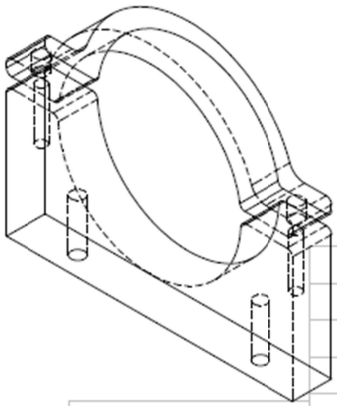

		UNLESS OTHERWISE SPECIFIED:		NAME	DATE
		DIMENSIONS ARE IN INCHES TOLERANCES: FRACTIONAL ± ANGULAR: MACH ± BEND ± TWO PLACE DECIMAL ± THREE PLACE DECIMAL ±	DRAWN	Z.B.	9/7/20
			CHECKED		
			ENG APPR.		
			MFG APPR.		
			Q.A.		
		INTERPRET GEOMETRIC TOLERANCING PER:	COMMENTS:		
		MATERIAL ALUMINUM			
NEXT ASSY	USED ON	FINISH MILLED			
APPLICATION		DO NOT SCALE DRAWING			

TITLE:

SIZE	DWG. NO.	REV
A	CLAMPS FOR COKING PROJECT	2
SCALE: 1:2	WEIGHT:	SHEET 1 OF 1

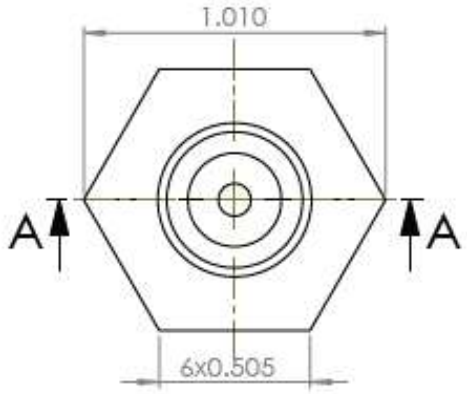
1.010
A
A
6x0.505

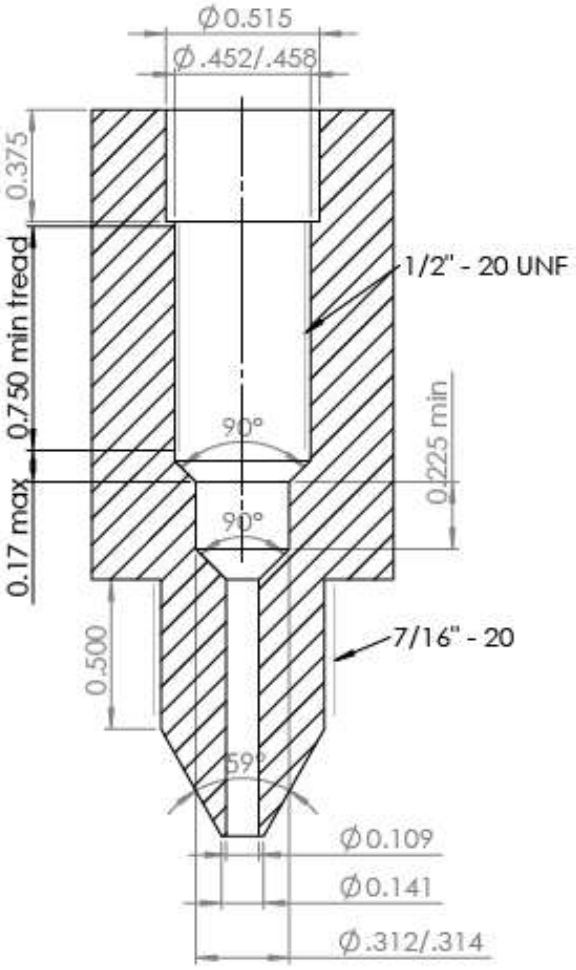
Ø0.515
Ø.452/.458
0.375
0.750 min tread
0.17 max
1/2" - 20 UNF
90°
0.225 min
90°
7/16" - 20
0.500
59°
Ø0.109
Ø0.141
Ø.312/.314

SECTION A-A

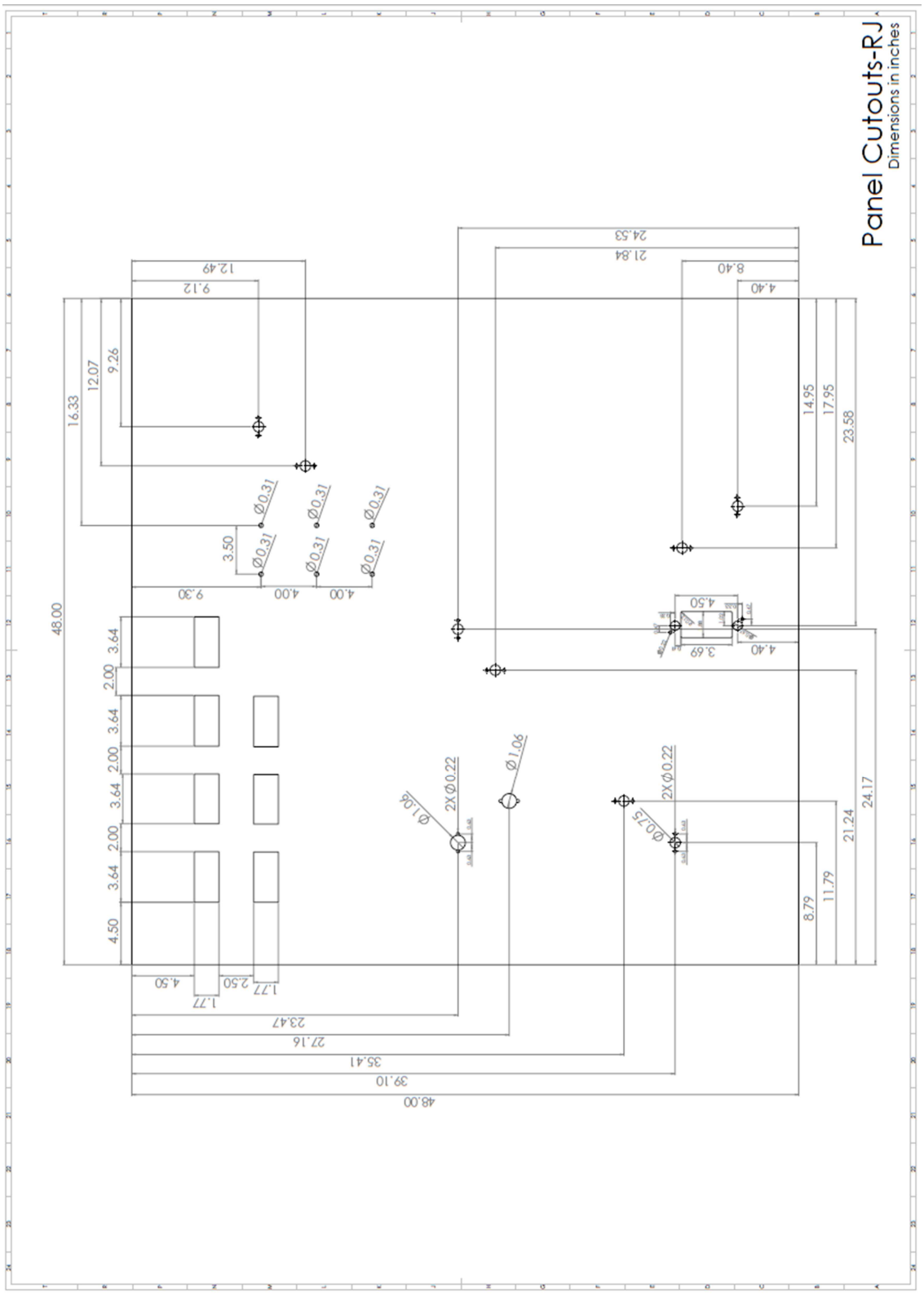
Panel Cutouts-RJ
Dimensions in inches
48.00
39.10
35.41
27.16
23.47
24.53
21.84
12.49
9.12
8.40
4.40
16.33
12.07
9.26
14.95
17.95
23.58
24.17
21.24
11.79
8.79
4.50
3.64
2.00
3.64
2.00
3.64
2.00
3.64
4.50
3.50
9.30
4.00
4.00
4.50
3.69
4.40
4.50
2.50
1.77
1.77
Ø0.31
Ø0.31
Ø0.31
Ø0.31
Ø0.31
Ø0.31
2XØ0.22
Ø1.06
Ø0.12
2XØ0.22
Ø0.75